Instituto Nacional de Astrofísica, Optica y Electrónica.

COHERENT MICRORING PERFECT ABSORBER

By

Enrique Sánchez Cristobal

A dissertation submitted in partial satisfaction of the requirements for the degree of

Master in Sciences,
with the specialty in optics

Supervised by: Dr. Dr. J. Javier Sánchez-Mondragón
Dr. Mercedeh Khajavikhan
Dr. Daniel A. May Arrioja

Mayo 2015, TONANTZINTLA, PUEBLA

TABLE OF CONTENTS

Page

LIST OF TABLES

Table **Page**

LIST OF FIGURES

Figure **Page**

1 INTRODUCTION

Time reversal symmetry is a basic concept in physics. It implies that if a particular physical process is allowed, then there also exist a "time reversed process" that is related to the original process by reversing momenta and the direction of certain fields. These symmetry operations are equivalent to change the sign of the time variable in the dynamical equations, and for the case of steady state they correspond to interchanging incoming and outgoing fields.

Based on everyday life observations, time reversal symmetry does not seem too obvious in real life. It always seems that all events occur in one direction in time. For example a movie, whether you run it forward or backward, of two billiard balls colliding and moving off at different speeds and different directions is consistent with Newton's laws. At least it would have time reversal symmetry if the friction between the billiard balls and the surface they are rolling on is negligible. The friction arises from process that cannot be reversed in time under typical experimental conditions. Thus friction breaks time reversal symmetry.

Maxwell's equations describing the propagation of waves in vacuum have the same time reversal symmetry as frictionless mechanics. But when in the presence of matter, interactions between the radiation and the medium play the same role as friction. Absorption violates the time reversal symmetry. However, the equations that describe the propagation of electromagnetic radiation in the presence of matter show a more general form of symmetry that relates two different process: absorption and emission.

Humans have learned to use amplifying devices that may reverse the effects of uniform losses in the propagation of electromagnetic waves. An electromagnetic amplifier is used to reverse the effects of uniform losses due to the propagation medium. The first amplifiers where in the range of radio frequencies (RF), eventually scientist learned how to amplify microwaves and optical radiation and the concept of maser and laser was introduced.

This ability of amplifiers to reverse the effects of electromagnetic losses points to a generalization of the time reversal symmetry: given an electromagnetic process in which a propagating electromagnetic wave is uniformly amplified to certain degree, there is a time reversed process with the same degree of absorption [1].

The most famous optical amplifier is the laser. In the laser oscillation process, a gain medium embedded in an optical cavity is subjected to an energy flux (the pump). When a threshold value of the pump is reached, it causes the emission of coherent electromagnetic radiation. The emitted radiation that escapes from the cavity does in the form of outgoing monochromatic waves. The emitted radiation field has a specific frequency and spatial distribution and it is generated without the need of an input field.

Therefore, by the generalized time reversal symmetry of electromagnetism; it should be possible to generate a field that will be perfectly absorbed if it has the same frequency and spatial distribution as the emitted laser field but be incoming rather that outgoing and the gain medium must be replaced by a medium that absorbs at the same rate that the laser’s gain medium amplifies.

A device acting as a time-reversed laser is termed a Coherent Perfect Absorber (CPA) or just an antilaser [2]. Actually the absorbing medium needs not to be strongly absorbing. The time reversed laser, the CPA, works as a perfect interference trap for radiation with a specific frequency and spatial distribution. So even if light can travel a long distance in the absorbing medium before it is absorbed, it will eventually get absorbed as it bounces back and forth indefinitely. On the other hand, a different radiation pattern will not be totally absorbed because the interference trap will not be created, in that case, a weakly absorbing medium will allow most of the light to scape even if the radiation pattern has the same frequency as the fully absorbed one. Highlighting this characteristic, one can consider tuning the external field to either enhance or suppress absorption.

The CPA concept idea has received great interest and stimulated theoretical and experimental studies. In reference [3], time reversal lasing and interferometric control of absorption was reported. Where a silicon wafer acting as a Fabry-Perot etalon illuminated from both sides with two counterpropagating coherent beams was used. Whereas in reference [4], a device acting as a laser oscillator and as an absorber has been proposed using the concepts of CPA and parity-time (PT) symmetry.

An extension of the time reversed laser concept and CPA has been suggested [5] for plasmonics nanostructures. Here coherent light is completely absorbed by matching the frequency and field pattern to that of a localized surface plasmon resonances.

A device that allows focusing radiation at nanoscale regions using the concept of coherent perfect nanoabsorbers based on the properties

of a slab with negative refraction and small loses was proposed in reference [6].

As expected, the CPA concept also has attracted research interest into different fields like plasmonics [5, 7, 8, 9, 10, 11, 12], graphene optics [13, 14, 15], acoustic waves [16], terahertz optics [17, 18], photonics crystals [17, 19, 20], and quantum optics [21, 22], in the latter for example the possibility of absorbing single photons was investigated.

Among the applications found for the CPA the more prominent are in integrated optical circuits where they may be used as optical modulators, transducers, detectors, and optical switches based on silicon (Si) waveguide or ring resonator technology [23, 24, 25].

Integrated optical circuits based on Si technology are quite promising for the new technological era [26]. The demonstration of a large number of ultracompact high-performance photonic components, overcoming the traditional limitations of silicon photonics, has been enabled by the progress in the nanofabrication techniques. Silicon based microring resonators are a key building used to perform many optical functions in silicon photonics networks

This technological era requires more sophisticated devices that can implement optical functions in a small scale with the aim of use them in integrated photonic networks. Taking advantage of the potential of the CPA and the versatility of silicon photonics technology in this work we investigate the design, simulation, fabrication, and characterization of a Coherent Perfect Absorber device based on an SOI microring resonator coupled to optical waveguides.

This work is divided in five chapters, chapter II provides the theoretical foundations to describe an optical resonator. The theoretical background of microring resonators coupled to optical waveguides using the matrix formalism of coupled mode theory is presented in chapter III. In Chapter IV the design and the fabrication process flow of the device is explained. The characterization setup and process of the fabricated device is detailed in chapter V including the results. Finally, the conclusions are given in chapter VI.

2 OPTICAL RESONATORS.

The optical resonator characteristics are briefly discussed. The Fabry Perot cavity is treated as a classical electromagnetic problem, then with this approach the basic parameters describing an optical resonator are derived. Subsequently, we analyze a slab cavity with two incident beams on both sides. This problem set the basis to understand the so called coherent perfect absorber that will be treated on next chapters.

2.1 The optical resonator.

An optical resonator, resonating cavity or optical cavity, the optical counterpart of an electronic resonant circuit is an arrangement of mirrors that confines and stores light at certain resonance frequencies. The simplest resonator comprises two parallel planar mirrors faced each other. Optical resonators are key components of lasers, surrounding the gain medium and providing feedback of the laser light. Light confined in the cavity reflect multiple times with little loss producing standing waves patterns at certain resonance frequencies. The produced patterns are called modes. In this chapter we examine the modes of the one dimensional simplest resonator better known as a Fabry-Perot etalon.

2.2 Resonant modes.

Consider the resonant cavity shown in Figure 2.1 and follow a wave as it bounces back and forth between the two mirrors. Looking the electric field just to the right of mirror 1 (M_1), labeled by $\mathbf{E}_0$, propagates to (M_2) and back to the starting plane experiencing and amplitude change of $\Gamma_1 \cdot \Gamma_2$ (Γ_1 and Γ_2 are the amplitude change caused by mirror 1 and mirror 2 respectively) and a phase factor $\exp[-ik2d]$ as it travels that round trip and

thus generates the field labeled $\mathbf{E}_1^+$, which experiences the same as $\mathbf{E}_0$ and generates $\mathbf{E}_2^+$, and so on. At every point along the path between the two mirrors, the fields $\mathbf{E}_1^+, \mathbf{E}_2^+$, and so on are to be added to $\mathbf{E}_0$ to which the reference phase 0° is assigned. This phasorial addition is shown in Figure 2.2 where because there is an assumed lagging phase angle, the round trip phase shift (RTPS), $2\theta = 2kd$, was assumed to be almost an integral multiple of 2π radians. That difference is labeled as ϕ and is related to kd by

$$2\theta = 2kd = m2\pi - \phi, \tag{2.1}$$

where m is an integer.

In a similar way, the total field $\mathbf{E}_T$ will be many times $\mathbf{E}_0$ if $\Gamma_1 \cdot \Gamma_2$ are almost 1 and $\phi = 0$. This is a very important point: the intensity of the

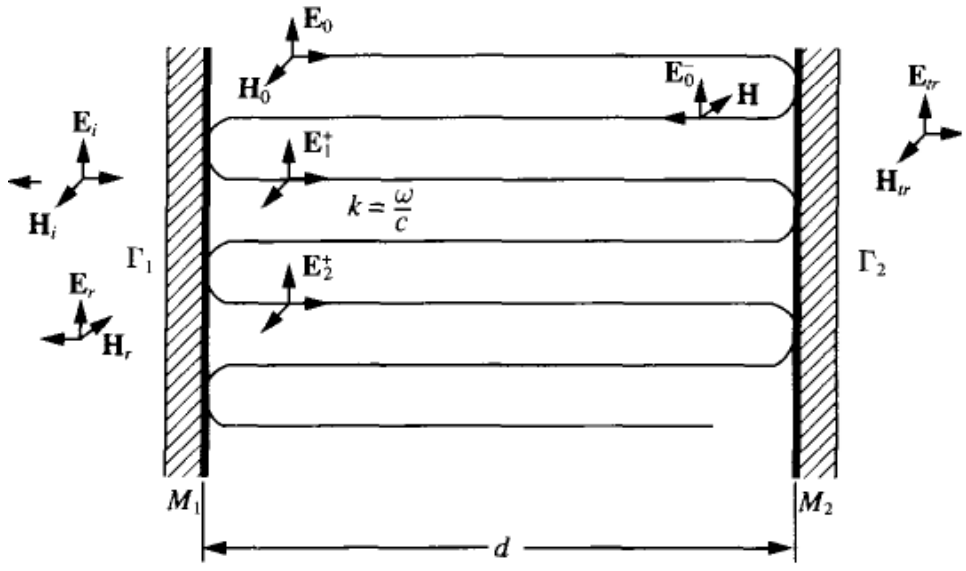

Figure 2.1. Optical cavity. (Figure extracted from reference **[36]**) Incident field shown at the right side of mirror 1 undergoes multiple bounces inside the cavity. At the right side of mirror 2 is shown the transmitted field. At the left part of mirror 1 is shown the reflected field traveling in the opposite direction as the incident field.

waves is maximized by the simple equation $\phi = 0,$ this physical fact is characteristic of resonance, and is defined as:

$$\text{round trip phase shift} = (\text{RTPS}) = 2kd = m2\pi\,, \tag{2.2}$$

looking at Equation (2.2) we can obtain a lot of interesting information.

As $k = \omega n / c = 2\pi / \lambda,$ c is the velocity of light in vacuum and n is the refractive index of the medium, we can use one of the equalities to find the resonant wavelengths

$$k \cdot 2d = \frac{\omega n \cdot 2d}{c} = \frac{2\pi \cdot 2d}{\lambda} = m \cdot 2\pi, \tag{2.3a}$$

$$d = \frac{m \cdot \lambda}{2}, \tag{2.3b}$$

where $\lambda = \lambda_0 / n.$ In this view of resonance that there has to be an integral number of half wavelengths between the two mirrors. This implies that the integer m is a very large number for optical frequencies.

We can also interpret Equation (2.2) in terms in the frequency ν

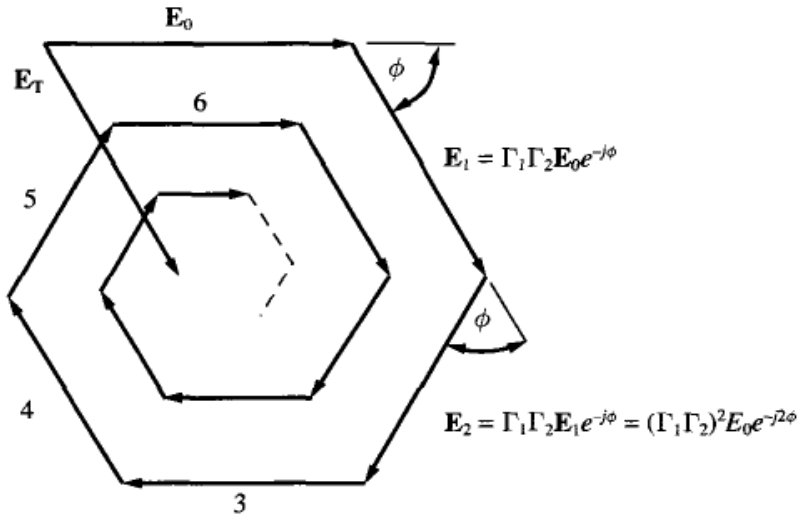

Figure 2.2. Phasor diagram. (Figure extracted from reference **[36]**)

$$k \cdot 2d = \frac{\omega \cdot 2nd}{c} = \frac{2\pi\nu \cdot 2nd}{c} = m(2\pi),$$
$$\nu = m \cdot \frac{c}{2nd}, \tag{2.4}$$

because m is restricted to integer values, there are only discrete frequencies which obey the resonance condition. The separation between those frequencies is given by

$$\nu_{m+1} - \nu_m = \frac{c}{2nd}. \tag{2.5}$$

2.3 *Q Factor and Finesse*

If we look again at Equation (2.2) it is obvious that the maximum internal field occurs at the resonance condition: $(\text{or RTPS} = m \cdot 2\pi),$ but what happens to the amplitude when there is a small deviation from the exact resonance condition? The issues to be addressed are (1) how small (2), what is the ratio of the fields at resonance to that at anti-resonance, and (3) what is the frequency selectivity of the cavity.

Three interrelated characteristic parameters associated with the cavity describe the resonance phenomenon: Q factor, F (finesse), and τ_p (photon lifetime). An analytic description of the fields inside the cavity and their relationship to those exciting the cavity is needed to derive an explicit relationship between the resonance, these quantities and the construction of the cavity.

The total electric field at the right side of mirror (M_1) and traveling to the right (indicated by the subscript "+") is given by the field E_0, which is the field transmitted through the mirror from the source, plus the fields that have made $(1 \text{ to } N)$ round trips to M_2, back to M_1, and starting the

$(2 \text{ to } N+1)$ trip. The amplitude of these fields are related to E_0 by the reflection coefficient of each mirror. The phase of the Nth component, E_N, is delayed with respect to E_0 by N times the round trip phase shift of $2kd = 2\theta$ and N times the phase contributed by each mirror[1]. For simplicity the last contribution is ignored

$$\begin{aligned} E_T^+ &= \sum E_N^+ = \mathbf{E}_0 \left\{ 1 + \Gamma_1 \Gamma_2 e^{-ik\cdot 2d} + \left(\Gamma_1 \Gamma_2 e^{-ik\cdot 2d} \right)^2 + \ldots \right\} \\ E_T^+ &= \mathbf{E}_0 \left[\frac{1}{1 - \Gamma_1 \Gamma_2 e^{-i2\theta}} \right], \end{aligned} \tag{2.6}$$

where θ is the optical length of the cavity $(\theta = \omega n d / c)$.

The total field traveling to the left returning from M_2 (indicated by the subscript "-") and incident on M_1 is just Γ_2 times E_T^+ times the round trip phase factor

$$E_T^- = \Gamma_2 e^{-i2\theta} E_T^+ = \mathbf{E}_0 \left[\frac{\Gamma_2 e^{-i2\theta}}{1 - \Gamma_1 \Gamma_2 e^{-i2\theta}} \right]. \tag{2.7}$$

Equations (2.6) and (2.7) state that the fields are a maximum when the denominators are a minimum $(\text{i.e., when } 2\theta = m \cdot 2\pi)$.

The intensity of the traveling waves I^+ and I^- are simply related to E^+ and E^- by $I = E \cdot E^* / 2\eta$[2]. For the right traveling wave we have:

$$I^+ \left(z = 0^+ \right) = \frac{\left| \mathbf{E}_0 \right|^2}{2\eta} \left\{ \left[\frac{1}{1 - \Gamma_1 \Gamma_2 e^{-i2\theta}} \right] \cdot \mathbf{E}_0 \left[\frac{1}{1 - \Gamma_1^* \Gamma_2^* e^{i2\theta}} \right] \right\}$$

[1] The phase of the reflection coefficient is usually a slow function of frequency, and here is neglected.

[2] η is the medium impedance.

$$I^+\left(z=0^+\right)=I_0\left\{\frac{1}{1-\Gamma_1^*\Gamma_2^* e^{i2\theta}-\Gamma_1\Gamma_2 e^{-i2\theta}+\left|\Gamma_1\Gamma_2\right|^2}\right\},$$

$$I^+\left(z=0^+\right)=I_0\frac{1}{1-2\left|\Gamma_1\Gamma_2\right|\cos 2\theta+\left|\Gamma_1\Gamma_2\right|^2},$$

$$I^+\left(z=0^+\right)=I_0\frac{1}{1-2\left|\Gamma_1\Gamma_2\right|\left[1-\sin^2\theta\right]+\left|\Gamma_1\Gamma_2\right|^2},$$

$$I^+\left(z=0^+\right)=I_0\frac{1}{1-2\left|\Gamma_1\Gamma_2\right|\left[1-\sin^2\theta\right]+\left|\Gamma_1\Gamma_2\right|^2},$$

$$\boxed{I^+\left(z=0^+\right)=\frac{E_0^2}{2\eta}\left\{\frac{1}{\left(1-\sqrt{R_1R_2}\right)^2+4\sqrt{R_1R_2}\sin^2\theta}\right\}}. \qquad (2.8)$$

Here we assume that the field reflection coefficients are real numbers and the power reflection coefficients have been substituted $R_{1,2}=\left|\Gamma_{1,2}\right|^2$. The reference plane $\left(z=0^+\right)$ is just to the right of the surface of M_1.

The quantity $E_0^2/2\eta$ is an intensity and is simply the power transmission coefficient of M_1 times the intensity $T_1\cdot E_{\text{inc}}^2/2\eta$, where $T_1=1-R_1$ for lossless mirrors. In a similar way the intensity transmitted through M_2 is the power transmission coefficient $T_2=1-R_2$ times the intensity given by Equation (2.8) with $z=d$. Converting to reflectivities and incident intensity, an expression for the intensity or power transmission coefficient through the two mirrors is obtained:

$$I_t=\left\{\frac{E_0^2}{2\eta}=T_1I_{\text{inc}}=\left(1-R_1\right)I_{\text{inc}}\right\}\left\{\frac{\left(1-R_2\right)}{\left(1-\sqrt{R_1R_2}\right)^2+4\sqrt{R_1R_2}\sin^2\theta}\right\}, \qquad (2.9)$$

or
$$T(\theta)=\frac{I_{\text{trans}}}{I_{\text{inc}}}=\left\{\frac{(1-R_1)(1-R_2)}{\left(1-\sqrt{R_1R_2}\right)^2+4\sqrt{R_1R_2}\sin^2\theta}\right\}. \qquad (2.10)$$

The net transmission is maximum when the denominator is a minimum. A plot of the transmission given by Equation (2.10) is shown in Figure 2-3, the horizontal axis is $[\theta/\pi-m]$.Thus it can be changed by varying the frequency $\omega=2\pi\nu$, the wavelength $\omega/c=2\pi/\lambda_0$, a distance d, or an index n. The vertical axes is the transmission coefficient but it can also serve as a measure of the relative fields, energy, or traveling intensities inside the cavity.

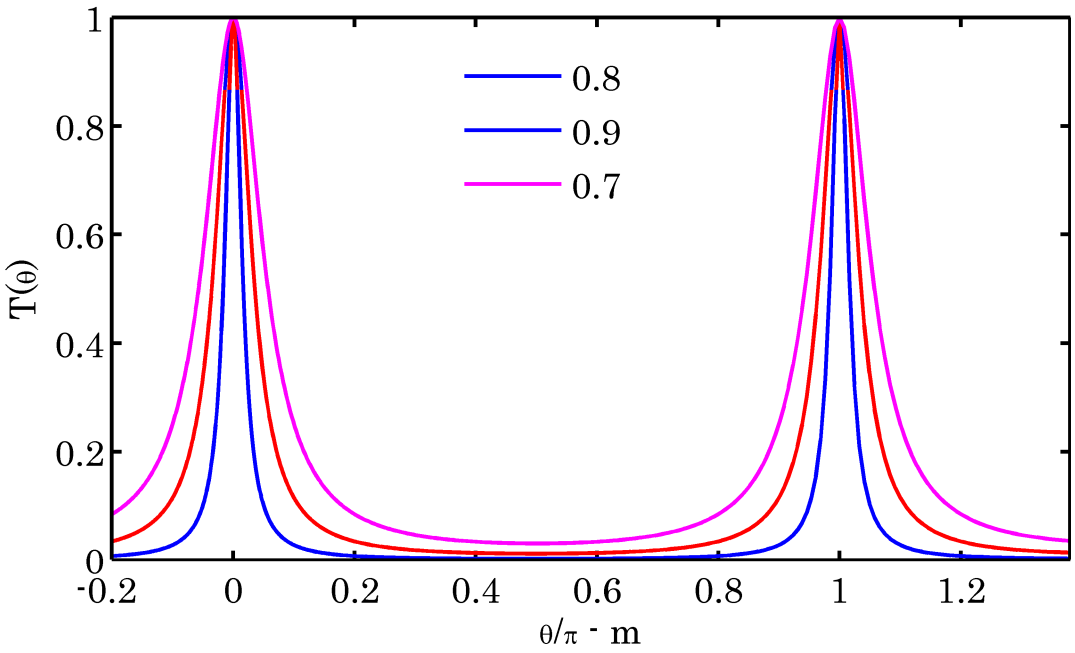

Figure 2.3. The transmission through a Fabry – Perot cavity as a function of the optical length in units of $\theta/\pi-m$ the three curves were plotted for $R_1=R_2=0.9, 0.8 \text{ and } 0.7.$

2.3.1 *Quality factor (Q)*

Under appropriate conditions the light can be "trapped" inside the optical resonator. In this particular case the optical beam becomes a mode of the resonator. A universal measure of this property is the quality factor of the resonator: Q.

The quality factor of the cavity is a measure of the sharpness or selectivity of the resonance. If ν_0 is the frequency of one resonance, then the Q is given by

$$Q = \frac{\nu_0}{\Delta\nu_{1/2}} = \frac{\omega_0}{\Delta\omega_{1/2}} = \frac{\lambda_0}{\Delta\lambda_{1/2}}, \tag{2.11}$$

where $\Delta\nu_{1/2}$ $\left(\Delta\lambda_{1/2}\right)$ is the full width at half maximum (FWHM). For reasonable values of the product of the reflectivities, one can expand $\sin\theta$ around the peak:

$$\sin\theta_{+,-} = \sin\left[\frac{\left(\omega_{+,-}\right)nd}{d}\right] = \pm\frac{1-\left(R_1R_2\right)^{1/2}}{\left(R_1R_2\right)^{1/4}}, \tag{2.12a}$$

and thus:

$$\Delta\nu_{1/2} = \nu_+ - \nu_- = \frac{c}{2nd}\left\{\frac{1-\left(R_1R_2\right)^{1/2}}{\pi\left(R_1R_2\right)^{1/4}}\right\}. \tag{2.12b}$$

Thus the cavity Q is given by $m\left(c/2nd\right)$ divided by $\Delta\nu_{1/2}$. We should recognize that m is merely the number of half wavelengths between the two mirrors; thus

$$Q = \frac{m\left(c/2nd\right)}{\Delta\nu_{1/2}} = \frac{2\pi nd}{\lambda_0}\frac{\left(R_1R_2\right)^{1/4}}{1-\left(R_1R_2\right)^{1/2}}, \tag{2.13}$$

since

$$m = \frac{nd}{\lambda_0/2}.$$

To provide a measure of the filtering properties of the cavity, one uses another term, the Finesse (F).

$$F = \frac{\text{free spectral range}}{\text{full width at half maximum}} = \frac{c/2nd}{\Delta\nu_{1/2}}, \tag{2.14}$$

or

$$F = \frac{\pi\left(R_1R_2\right)^{1/4}}{1-\left(R_1R_2\right)^{1/2}}. \tag{2.15}$$

2.4 *Photon Lifetime*

Related to the quality factor or the finesse F of a cavity is the photon lifetime. It is a time constant describing the build up or the decay of energy in a cavity and is one of the most useful parameters describing a cavity.

Consider Figure 2.4, which depicts a single cavity with a package of photons bouncing back and forth between the mirrors. Assuming that at $t=0$ there are N_p photons in this package. Hence, the energy in the cavity is $h\nu N_p$ .the number of photons surviving one round trip is $\left[S=R_1R_2\right]$ times the initial number of photons and thus the number lost is

$$\text{number of photons lost in one round trip} = \left[1-S\right]N_p. \tag{2.16}$$

The time rate of change of photons (or energy) in the cavity is given by the negative of the number lost divided by the time for the round trip $\left(\tau_{RT}\right)$

$$\frac{\Delta N_p}{\Delta t} \to \frac{dN_p}{dt} = \frac{N_p\left(t+\tau_{RT}\right)-N_p\left(t\right)}{\tau_{RT}} = -\frac{\left[1-S\right]N_p}{\tau_{RT}},$$

or

$$\frac{dN_p}{dt} \triangleq -\frac{N_p}{\tau_p}, \tag{2.17a}$$

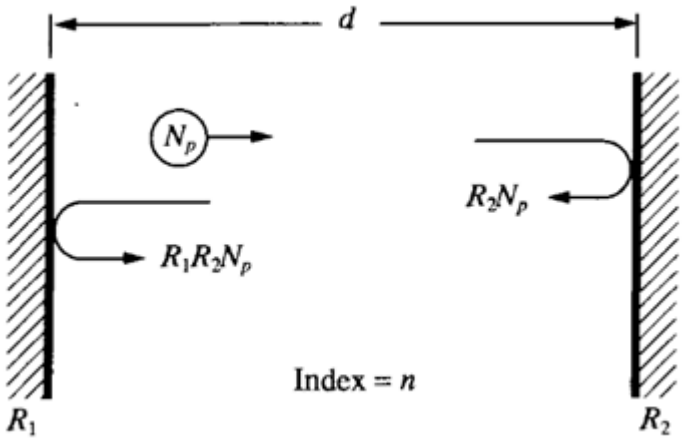

Figure 2.4. Decay of photons in a cavity. (Figure extracted from reference **[36]**)

where

$$\tau_p = \frac{\tau_{RT}}{1-S}, \tag{2.17b}$$

here τ_p is the photon lifetime.

Equation (2.17a) has a simple solution:

$$N_p(t) = N_p(0)e^{-t/\tau_p}. \tag{2.18}$$

Thus it takes on the order of $(1-S)^{-1}$ round trips for the stored photon energy to decrease to 36.8% $\left(=e^{-1}\right)$ of its initial value. For the cavity in Figure 2-4, $\tau_{RT} = 2nd/c$ and S is the product of the reflectivities.

The concept of photon life time is more important for the theoretical point of view and it can be related to Q by the theoretical definition of Q

$$Q = \frac{2\pi(\text{energy stored in the system at resonance = W})}{(\text{energy lost in a cycle of oscillation})}. \tag{2.19}$$

The energy lost in a cycle is the average power lost in one cycle times the period of oscillation:

$$Q = \frac{2\pi}{T} \cdot \frac{W}{\langle P \rangle} = \omega_0 \frac{W}{\langle P \rangle}. \tag{2.20}$$

The average power is equal to the time rate of change in the stored energy W.

$$Q = \omega_0 \frac{W}{-dW/dt},$$

$$\frac{dW}{dt} = -\frac{\omega_0}{Q} \cdot W, \tag{2.21}$$

rewriting the power in terms of the number of photons we have:

$$\frac{d\left[h\nu N_p\right]}{dt} = -\frac{\omega_0}{Q} \cdot \left[h\nu N_p\right] = -\frac{\left[h\nu N_p\right]}{\tau_p},$$

thus

$$\tau_p = \frac{Q}{\omega_0} \tag{2.22}$$

Equation (2.22) is the connection between the photon lifetime and the quality factor. Since $\Delta\omega_{1/2} = \omega_0 / Q$, we have the relationship:

$$\Delta\omega_{1/2} = \frac{1}{\tau_p},$$

or

$$\Delta\omega_{1/2}\tau_p = 1. \tag{2.23}$$

If we know the FWHM of the resonance $\Delta\lambda_{1/2} = \Delta\omega_{1/2} / 2\pi,$ the calculation of the Q factor or the Finesse is easy. For the example cavity:

$$\tau_p = \frac{\tau_{RT}}{1-S} = \frac{2nd/c}{1-R_1R_2}, \qquad \text{by (2.17b)}$$

and using Equation (2.23) we arrive to:

$$\Delta\lambda_{1/2} = \frac{1}{2\pi\tau_p} = \frac{c\left(1-R_1R_2\right)}{\left(2nd\right)\cdot 2\pi}. \tag{2.24}$$

If we use the definition of Q from Equation (2.13) and the definition of FWHM from the last equation we have:

$$Q = \frac{\nu_0}{\Delta\lambda_{1/2}} = 2\pi\nu_0\left(\frac{2nd}{c}\right)\frac{1}{1-R_1R_2} = \frac{4\pi nd}{\lambda_0}\left(\frac{1}{1-R_1R_2}\right), \tag{2.25}$$

and finally the finesse:

$$F = \frac{FSR}{\Delta\nu_{1/2}} = \frac{c/2nd}{\Delta\nu_{1/2}} = \frac{2\pi}{1-R_1R_2}. \tag{2.26}$$

The derived equations describe an optical cavity in the simplest case (Fabry-Perot) and are very useful in laser cavities design. There are three important issues regarding a cavity: (1) the resonant enhancement of the internal energy inside the cavity, (2) the spectral separation and selectivity of the resonances and (3) the integration constant τ_p associated with each resonance.

2.5 *Fabry-Perot cavity with two input beams.*

So far, we have analyzed a Fabry Perot cavity made of two facing mirrors, now we turn to a slab acting as a Fabry Perot cavity. This slab has the faces polished in a way that they act as two partial transmitting mirrors. The slab of thickness d has a complex refractive index $n = n_r + in_i$ and is immersed in a medium with real refractive index n_0, which is approximately 1 in air. In this analysis we consider two impinging beams, a left beam with electric field $E_L^{(i)}$ and a right beam with electric field $E_R^{(i)}$. Figure 2.5 depicts a schematic model of this situation. The electric fields are:

$$E_L^{(i)} = E^{(i)} e^{i(kz - \omega t + \varphi_L)} = A_L^{(i)} e^{i(kz - \omega t)}, \tag{2.27}$$

$$E_R^{(i)} = E^{(i)} e^{i(kz + \omega t + \varphi_R)} = A_R^{(i)} e^{i(kz + \omega t)}, \tag{2.28}$$

where $A_L^{(i)}$ and $A_R^{(i)}$ are complex amplitudes, ω is the angular frequency of light, k is the wave number $k = n_0 \omega / c,$ and c is the speed of light. The subscripts L and R stand for the left and right side of the cavity, respectively; and the suffixes i, r and t refer throughout to the incident, reflected and transmitted waves respectively. We assume that both beams have the same real amplitude $E^{(i)}$, polarized in the x direction, propagating in the $+z$ or $-z$ directions, with initial phase factors φ_L and φ_R for the left and right beams, respectively. All vectors are referred to the Cartesian coordinate system defined in Figure 2.5.

The problem of a light beam at normal incidence on a Fabry Perot cavity filled with a real refractive index medium has been treated in [27]. At the first interface, the incident beam is partially reflected by the slab face. The transmitted beam subsequently undergoes further reflections and transmissions in multiple round trips in the cavity ()as we saw in the previous section).At the left surface, the outgoing beam, propagating in $-z$ direction as shown in Figure 2.5, is the superposition of the reflected

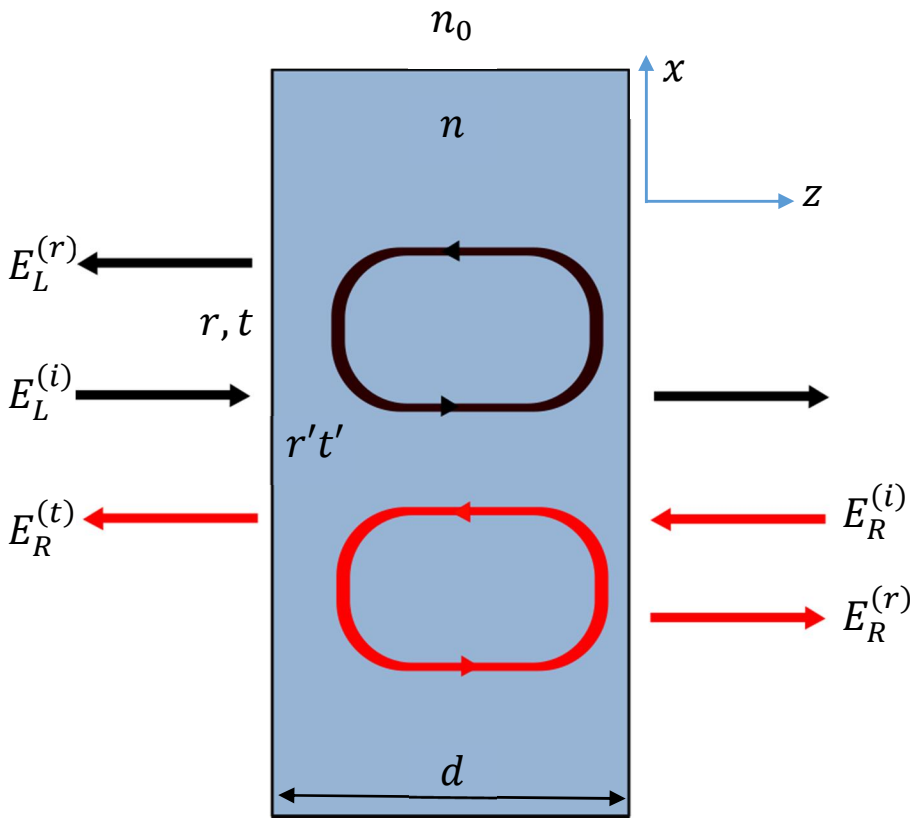

Figure 2.5. Fabry Perot cavity of thickness d and complex refractive index immersed in a medium of real refractive index. Two coherent beams impinging on both end surfaces are shown. Each incident wave causes a reflected and transmitted wave.

beam on the left surface and the transmitted beams originated from the left beam after multireflections, and the transmitted beams originating from the right beam after multireflections. The reflection and transmission coefficients at the left surface are r and t fro an external reflection and r' and t' for an internal reflection where the coefficients satisfy the following relations derived from [27]:

$$r = -r' = \frac{n_0 - n_r}{n_0 + n_r}, \quad t = \frac{2n_0}{n_0 + n_r}, \quad t' = \frac{2n_r}{n_0 + n_r}, \tag{2.29}$$

$$tt' + r^2 = tt' + r'^2 = tt' - rr' = 1, \tag{2.30}$$

where n_0 and n_r are the real parts of the refractive indices of the surrounding medium and the slab, respectively. For semiconductors, such as silicon, n_r is dispersive and depends on the doping concentration. As

the beam traverses through the slab, the phase shift θ after each round trip in the cavity, is given by:

$$\theta = \frac{4\pi n_r d}{\lambda_0},$$

where λ_0 is the wavelength in free space. When the cavity filled with an absorbing medium, an imaginary part of the refractive index must be included and the round trip phase shift becomes a complex number:

$$\theta = \frac{4\pi nd}{\lambda_0} = \theta_1 + i\theta_2 = \frac{4\pi n_r d}{\lambda_0} + i\frac{4\pi n_i d}{\lambda_0}, \tag{2.31}$$

where θ_1 stands for a phase shift caused by the real part of the refractive index n_r and θ_2 stands for the round trip absorption caused by the imaginary part of the refractive index n_i. The electric field of the reflected beam, originated from the left beam, is the sum of the reflected wave on the left surface, and transmitted beams originated from the left beam after multiple reflections in the slab. $E_L^{(r)}$ can be expressed as

$$E_L^{(r)} = E^{(r)} e^{-i(kz+\omega t+\varphi_L)} = A_L^{(r)} e^{-i(kz+\omega t)}, \tag{2.32}$$

where $A_L^{(r)}$ is given as [27]

$$A_L^{(r)} = \frac{\left(1-e^{i\theta}\right)r}{1-r^2 e^{i\theta}} A_L^{(i)}. \tag{2.33}$$

At the left surface, there will be another contribution to the outgoing beam originated from the right beam after multiple reflections in the cavity, whose electric field is given by:

$$E_R^{(t)} = E^{(t)} e^{-i(kz+\omega t+\varphi_R)} = A_R^{(t)} e^{-i(\omega t-kz)}, \tag{2.34}$$

$$A_R^{(t)} = \frac{tt'}{1-r^2 e^{i\theta}} A_R^{(i)} e^{i\frac{\theta}{2}}, \tag{2.35}$$

where the term $e^{i\frac{\theta}{2}}$ represents the phase shift and absorption in a single pass to correctly describe the phase relation between beams originated from the left and right beams.

The total amplitude of the outgoing beam, $A_{\text{Left}}^{(\text{total})}$, propagating towards the left, is the coherent addition of $E_L^{(r)}$ and $E_R^{(t)}$:

$$A_{\text{Left}}^{(\text{total})} = \frac{\left(1-e^{i\theta}\right)r}{1-r^2e^{i\theta}} A_L^{(i)} + \frac{tt'}{1-r^2e^{i\theta}} A_R^{(i)} e^{i\frac{\theta}{2}}, \tag{2.36}$$

similarly, the total amplitude $A_{\text{Right}}^{(\text{total})}$, propagating towards the right is:

$$A_{\text{Right}}^{(\text{total})} = \frac{\left(1-e^{i\theta}\right)r}{1-r^2e^{i\theta}} A_R^{(i)} + \frac{tt'}{1-r^2e^{i\theta}} A_L^{(i)} e^{i\frac{\theta}{2}}, \tag{2.37}$$

with:

$$A_L^{(i)} = E^{(i)}e^{i\varphi_L}, \quad A_R^{(i)} = E^{(i)}e^{i\varphi_R}$$

Equation (2.36) becomes

$$A_{\text{Left}}^{(\text{total})} = \frac{E^{(i)}}{1-r^2e^{i\theta}}\left[\left(1-e^{i\theta}\right)re^{i\varphi_L} + tt'e^{i\varphi_R}e^{i\frac{\theta}{2}}\right], \tag{2.38}$$

$$A_{\text{Left}}^{(\text{total})} = \frac{E^{(i)}e^{i\varphi_L}}{1-r^2e^{i\theta}}\left[\left(1-e^{i\theta}\right)r + tt'e^{i\Delta}e^{i\frac{\theta}{2}}\right], \tag{2.39}$$

and Equation (2.37)

$$A_{\text{Right}}^{(\text{total})} = \frac{E^{(i)}e^{i\varphi_R}}{1-r^2e^{i\theta}}\left[\left(1-e^{i\theta}\right)r + tt'e^{-i\Delta}e^{i\frac{\theta}{2}}\right], \tag{2.40}$$

where $\Delta = \varphi_R - \varphi_L$.

When the phase difference is 0, even mode, the two beams are in phase, and the thickness d satisfices the relation $n_r d = m\lambda_0$, where m is an integer. For the odd mode the two beams are out of phase, $\Delta = \varphi_R - \varphi_L = \pi$, and the thickness d satisfices the relation $n_r d = \left(m+\frac{1}{2}\right)\lambda_0$, where m is an integer.

In both cases, $A_{\text{Left}}^{(\text{total})}$ is

$$A_{\text{Left}}^{(\text{total})} = \frac{E^{(i)} e^{i\varphi_L}}{1 - r^2 e^{-\theta_2}} \left[\left(1 - e^{-\theta_2}\right) r + tt' e^{-\frac{\theta_2}{2}} \right], \tag{2.41}$$

If the numerator goes to zero, the outgoing light is completely extinguished. For this to happen, is required that:

$$-\left(1 - e^{-\theta_2}\right) r = tt' e^{-\frac{\theta_2}{2}} = \left(1 - rr'\right) e^{-\frac{\theta_2}{2}} \tag{2.42}$$

The solution for Equation (2.42) is:

$$\theta_2 = -2\ln(-2) = 2\ln\left(\frac{n_r + n_0}{n_r - n_0}\right), \tag{2.43}$$

then, we have the next condition for the imaginary part of the refractive index to fully extinguish the outgoing wave:

$$n_i = \frac{1}{kd} \ln\left(\frac{n_r + n_0}{n_r - n_0}\right). \tag{2.44}$$

Because of the symmetry, the total amplitude $A_{\text{Right}}^{(\text{total})}$ at the right surface also vanishes as $A_{\text{Left}}^{(\text{total})}$ vanishes.

The above analysis shows an important result that a slab with a complex refractive index n and thickness d becomes a **coherent perfect absorber** operating in the even or odd modes when the imaginary part of the slab refractive index satisfies Equation (2.44). Such a device will be explained for a ring geometry in a subsequent chapter.

We have derived the basics parameters whose describe an optical cavity, then we analyzed a cavity made of a slab with complex refractive index and found that for certain values of the imaginary part the outgoing radiation is fully extinguished.

3 MICRORING RESONATORS.

We describe an optical cavity which is made of a microring resonator and derive all its parameters. Two important geometries are studied, microring resonator coupled to one optical waveguide and a microring laterally coupled to two optical waveguides. Both configurations are analog to those presented in previous chapter.

3.1 Microring resonators.

A ring resonator is formed by placing three mirrors in a triangular geometry, when light is reflected in each mirror it forms a closed path. A straight waveguide bent in a circular form makes a ring resonator, if the radius of the formed ring is in the order of microns it is called *micro-ring resonator* [27]. When a ring resonator is placed close enough to a waveguide through which a light beam propagates, the light is transferred to the ring via evanescent field and therefore will travel around the ring. If the light accumulates a phase shift equal to an integer multiple of 2π in each full trip around the close loop it will constructively interfere. The frequency of this light is then the resonance frequency of the micro-ring. Light that does not meet this resonance condition will be coupled back to the waveguide without undergoing any change. From another point of view, a ring resonator is nothing but a filter that captures light meeting the resonant condition keeping unchanged light which does not meet this condition. A micro ring resonator is a frequency-selective device. Ideally a ring resonator only selects light of single frequency, deviations from this ideal behavior are described by the ring Q factor.

This frequency-selective characteristic makes the micro ring resonators useful as building blocks for a variety of integrated photonic devices such as filters, switches, modulators, detectors, and laser cavities. In this work a micro ring resonator will be used as a cavity for a coherent perfect absorber. The low bending loss of SOI (Silicon on Insulator) based waveguides and its high index contrast has made them very promising for the fabrication of micro-ring resonators with smaller radius and also to couple light into them with high efficiency [26]. In addition, advanced fabrications techniques such as electron beam lithography (e-beam lithography) make possible the fabrication of rings with a width waveguide of about a hundred of nanometers which could not be achieved with conventional optical lithography due to the diffraction limit. This makes the SOI-based technology the most appropriate to fabricate integrated photonic circuits on micro and nano scale which can perform complex tasks.

This chapter gives an introduction to the theory of ring resonators using the coupled mode theory matrix formalism [28]. Two basic geometries are considered, micro-ring coupled to a waveguide and micro ring coupled to two waveguides and then the parameters that help to characterize the resonator are obtained.

A microring-resonator is an optical cavity that has a resonant frequency spectrum that is dependent of the size. Manipulating the coupling of optical waveguides and microring resonators is an important area of research and development [26], the basic configuration consist in a bus waveguide coupled via evanescent field to a microring resonator. To analyze this geometry we consider the region where power exchange between the waveguide and the micro resonator takes place. If we consider that the coupling is lossless and that a single unidirectional mode of the resonator is excited (no reflection takes

place) then the coupling can be described by means of the unitary coupling matrix:

$$\begin{pmatrix} b_1 \\ b_1' \end{pmatrix} = \begin{pmatrix} \tau & \kappa \\ -\kappa^* & \tau^* \end{pmatrix} \begin{pmatrix} a_1 \\ a_1' \end{pmatrix}, \tag{3.1}$$

$$|\tau|^2 + |\kappa|^2 = 1, \tag{3.2}$$

where κ is the coupling factor and τ is a coupling parameter. a_1, a_1' are the mode amplitudes at the input of the coupling area and b_1, b_1' are the amplitude at the output. The complex mode amplitudes are normalized such that their square magnitude corresponds to the modal power. The specific form of κ depends on the coupling mechanism employed, here the coupling of modes mechanism is used and the derivation of the coupling factor κ is shown in appendix A.

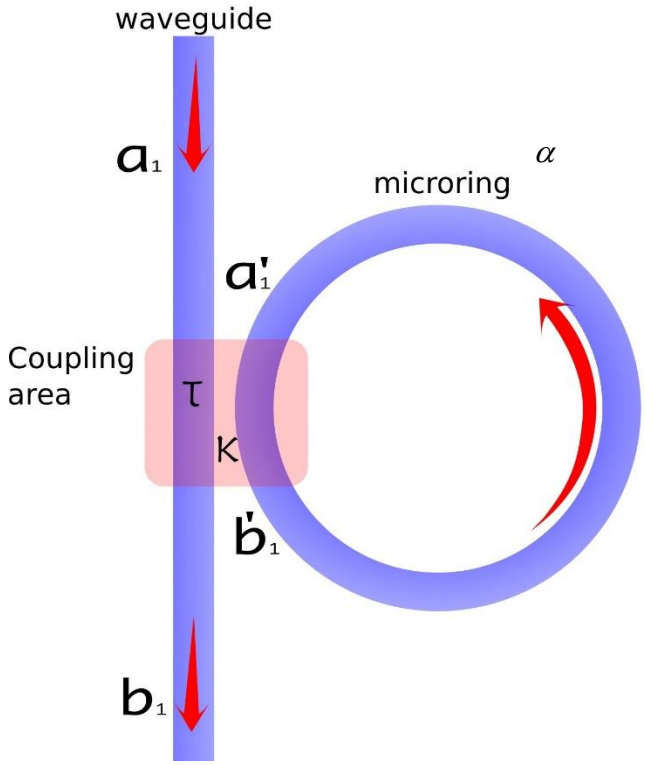

Figure 3.1 Microring resonator coupled to an optical waveguide, input, output, and circulating waves are indicated with red arrows. The coupling region is marked with a gray box, in this area the role of the coupling parameters takes place.

The round trip in the ring is given by

$$a_1' = \alpha e^{i\phi} b_1', \tag{3.3}$$

where α is the attenuation factor, is real. For zero internal loss $\alpha = 1.$ ϕ is the total phase accumulated when light travels around the ring $\phi = 2\pi R k_0 n_{eff}$, R being the radius of the ring measured from the center of the ring to the center of the waveguide, n_{eff} is the effective index and k_0 is the vacuum wavenumber. The propagation constant is $\beta = k_0 n_{eff}$. From Equation (3.1) we have:

$$b_1 = \tau a_1 + \kappa a_1', \tag{3.4}$$

$$b_1' = -\kappa^* a_1 + \tau^* a_1'. \tag{3.5}$$

Using Equation (3.3) into Equation. (3.4) and solving for b_1' we obtain:

$$b_1' = -k^* a_1 + \tau^* \left(\alpha e^{i\phi} b_1'\right),$$

$$b_1' = \frac{-k^* a_1}{1 - \tau^* \alpha e^{i\phi}}, \tag{3.6}$$

now, using Equation (3.6) in Equation (3.3) and substituting into Equation (3.4) we arrive to:

$$b_1 = \tau a_1 + \kappa\left(\alpha e^{i\phi} b_1'\right),$$

$$b_1 = \tau a_1 + \kappa\left[\alpha e^{i\phi}\left(\frac{-k^* a_1}{1 - \tau^* \alpha e^{i\phi}}\right)\right],$$

$$b_1 = \frac{\tau a_1 - a_1 \alpha e^{i\phi}\left(|\tau|^2 + |\kappa|^2\right)}{1 - \tau^* \alpha e^{i\phi}},$$

using Equation (3.2) in the last equation and multiplying for $e^{-i\phi} / e^{-i\phi}$ we have:

$$b_1 = \frac{-\alpha + \tau e^{-i\phi}}{-\tau^* \alpha + e^{-i\phi}} a_1. \tag{3.7}$$

The transmission factor in the input waveguide is given by:

$$\left|\frac{b_1}{a_1}\right|^2 = \frac{\alpha^2 + |\tau|^2 - 2\alpha|\tau|\cos(\phi+\varphi_\tau)}{1+|\tau|^2\alpha^2 - 2\alpha|\tau|\cos(\phi+\varphi_\tau)}, \tag{3.8}$$

where $\tau = |\tau|\exp(i\varphi_\tau)$, $|\tau|$ represents the coupling losses and φ_τ is the coupling phase.

Similarly, using Equation (3.3) and Equation (3.6) we obtain:

$$a_1' = \frac{-\alpha\kappa^*}{-\alpha\tau^* + e^{-i\phi}}a_1, \tag{3.9}$$

$$\left|\frac{a_1'}{a_1}\right|^2 = \frac{\alpha\left(1-|\tau|^2\right)}{1+\alpha|\tau|^2 - 2\alpha|\tau|\cos(\phi+\varphi_\tau)}. \tag{3.10}$$

In Equation (3.10), $|a_1'|^2$ is the total circulating power around the ring. In the above equations $|a_1'|^2$ and $|b_1|^2$ are the respective traveling wave power. For simplicity we can set the input power $|a_1|^2$ equal to unity, that is to have normalized output intensities.

The most interesting features of this resonator occur near resonance, that is $(\phi+\varphi_\tau) = 2m\pi$, m being an integer, Equation (3.8) and (3.10) become:

$$|b_1|^2 = \frac{(\alpha-|\tau|)^2}{(1-\alpha|\tau|)^2}, \tag{3.11}$$

$$|a_1'|^2 = \frac{\alpha\left(1-|\tau|^2\right)}{(1-\alpha|\tau|)^2}. \tag{3.12}$$

Equation (3.11) is of special interest. It shows that when the internal losses are equal to the coupling losses i.e. $\alpha = |\tau|$, the transmission power vanishes $\left(|b_1|^2 = 0\right)$. This particular condition is known as critical coupling. Critical coupling is due to destructive

interference between the transmitted wave in the waveguide τa_1 and the internal field coupled to the input waveguide $\kappa a_1'$.

Using the equations obtained one can have a good idea of the behavior of a micro ring resonator coupled to a waveguide. Figure 3.2 shows the frequency selective characteristic of a micro ring with a radius of 150 μm. the parameters were obtained with the derived expressions. Two frequencies where the transmission is zero (resonance frequencies) are observed indicating that we are in the critical coupling condition for that frequencies.

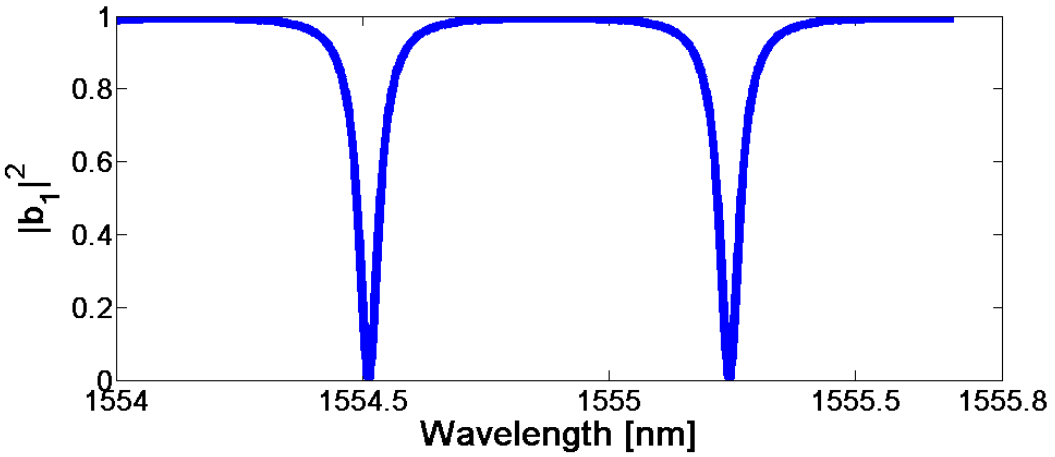

Figure 3.2 Microring resonator optical spectral response.

3.2 *Microring resonator coupled to two optical waveguides.*

Another geometry of special interest is when two waveguides are coupled to the micro ring resonator, a schematic is shown in Figure 3.3. Using the same matrix method used above we can deduce the amplitudes of the waves outgoing from the waveguides:

$$\begin{pmatrix} b_1 \\ b_1' \end{pmatrix} = \begin{pmatrix} \tau_1 & \kappa_1 \\ -\kappa_1^* & \tau_1^* \end{pmatrix} \begin{pmatrix} a_1 \\ a_1' \end{pmatrix}, \tag{3.13}$$

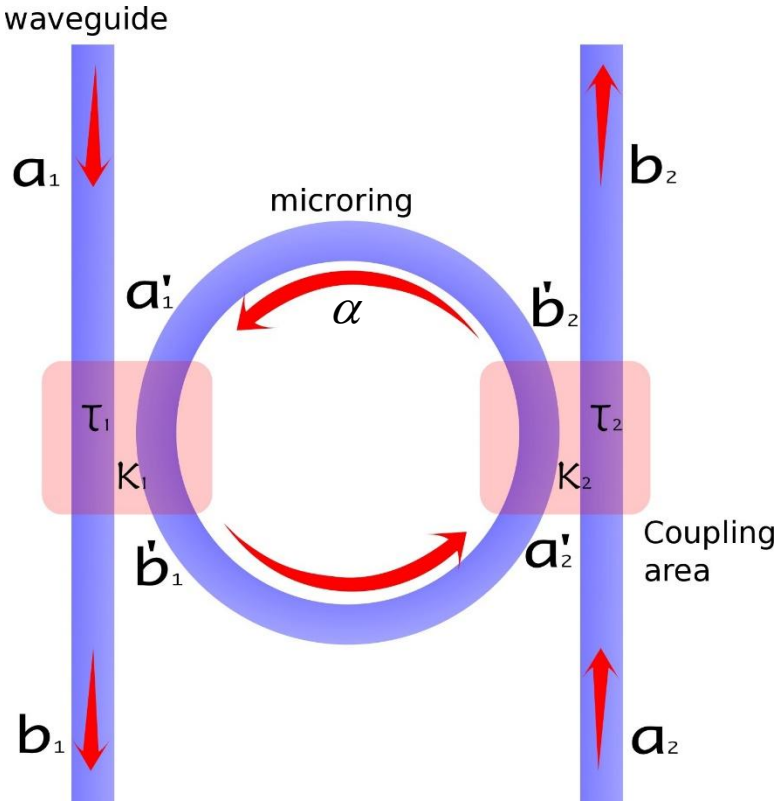

Figure 3.3. Microring resonator coupled to two optical waveguides

$$\begin{pmatrix} b_2' \\ b_2 \end{pmatrix} = \begin{pmatrix} \tau_2^* & \kappa_2 \\ -\kappa_2^* & \tau_2 \end{pmatrix} \begin{pmatrix} a_2' \\ a_2 \end{pmatrix}, \qquad (3.14)$$

the following relationships between the couplers are valid,

$$|\tau_1|^2 + |\kappa_2|^2 = 1, \qquad (3.15)$$

$$|\tau_2|^2 + |\kappa_2|^2 = 1, \qquad (3.16)$$

the field amplitudes inside the ring are related by

$$a_2' = \alpha^{1/2} e^{i\phi/2} b_1', \qquad (3.17)$$

$$a_1' = \alpha^{1/2} e^{i\phi/2} b_2', \qquad (3.18)$$

where $\alpha^{1/2}$ and $e^{i\phi/2}$ are the half round trip loss and phase respectively. In order to have a transmission in the second waveguide, the mode circulating around the ring must pass the second coupler. For simplicity the amplitude of the input wave can be unitary and we consider a zero

input field i.e. $a_2 = 0$. Using the above expressions we can obtain the field amplitudes for the outgoing and circulating waves:

$$b_1 = \frac{\tau_1 - \tau_2^* \alpha e^{i\phi}}{1 - \tau_1^* \tau_2^* \alpha e^{i\phi}} a_1, \tag{3.19}$$

$$a_1' = \frac{-\tau_2^* \kappa_1^* \alpha e^{i\phi}}{1 - \tau_1^* \tau_2^* \alpha e^{i\phi}} a_1, \tag{3.20}$$

$$b_2 = \frac{\kappa_1^* \kappa_2^* \alpha^{1/2} e^{i\phi/2}}{1 - \tau_1^* \tau_2^* \alpha e^{i\phi}} a_1. \tag{3.21}$$

If we normalize the mode amplitudes then the square magnitude corresponds to the modal power. The power at the output of each waveguide and the circulating power is:

$$|b_1|^2 = \frac{|\tau_1|^2 - 2|\tau_1||\tau_2|\alpha\cos\phi + |\tau_2|^2 \alpha^2}{1 - 2|\tau_1||\tau_2|\alpha\cos(\phi - \theta_1 - \theta_2) + |\tau_1|^2 |\tau_2|^2 \alpha^2}, \tag{3.22}$$

$$|a_1'|^2 = \frac{|\tau_2|^2 \left(1 - |\tau_1|^2\right)\alpha^2}{1 - 2|\tau_1||\tau_2|\alpha\cos(\phi - \theta_1 - \theta_2) + |\tau_1|^2 |\tau_2|^2 \alpha^2}, \tag{3.23}$$

$$|b_2|^2 = \frac{\left(1 - |\tau_2|^2\right)\left(1 - |\tau_1|^2\right)\alpha^2}{1 - 2|\tau_1||\tau_2|\alpha\cos(\phi - \theta_1 - \theta_2) + |\tau_1|^2 |\tau_2|^2 \alpha^2}, \tag{3.24}$$

where we have considered $\tau_i = |\tau_i| e^{i\theta_i}$, θ_i with $(i = 1,2)$ is the phase change in each coupler.

Considering the case of resonance $(\phi - \theta_1 - \theta_2) = 2m\pi$ the following expressions are obtained:

$$|b_1|^2 = \frac{\left(|\tau_1| - \alpha|\tau_2|\right)^2}{\left(1 - |\tau_1||\tau_2|\alpha\right)^2}, \tag{3.25}$$

$$|a_1'|^2 = \frac{|\tau_2|^2 \left(1 - |\tau_1|^2\right)\alpha^2}{\left(1 - |\tau_1||\tau_2|\alpha\right)^2}, \tag{3.26}$$

$$|b_2|^2 = \frac{\left(1-|\tau_2|^2\right)\left(1-|\tau_1|^2\right)\alpha^2}{\left(1-|\tau_1||\tau_2|\alpha\right)^2}. \qquad (3.27)$$

Looking at Equation (3.24), the transmission power at the upper waveguide is zero when the following conditions are fulfilled: $\alpha = 1$ (zero internal losses) and $|\tau_1| = |\tau_2|$ in this case $|b_1|^2 = 0$ and $|b_2|^2 = 1$ what means that all the input power is transferred to the lower waveguide. In practice achieving zero internal loss implies incorporating a sort of gain in the ring. Typically α is less than unity, in this case for achieving a full transfer power to the lower waveguide the condition, $\alpha = |\tau_1| / |\tau_2|$ must be satisfied. The so called critical coupling condition is only satisfied with asymmetric coupling. Figure 3.4 shows the output at the two waveguides of this geometry. As we observe, when the power at the upper waveguide drops the power at the lower waveguide is maximum, this is the critical coupling condition.

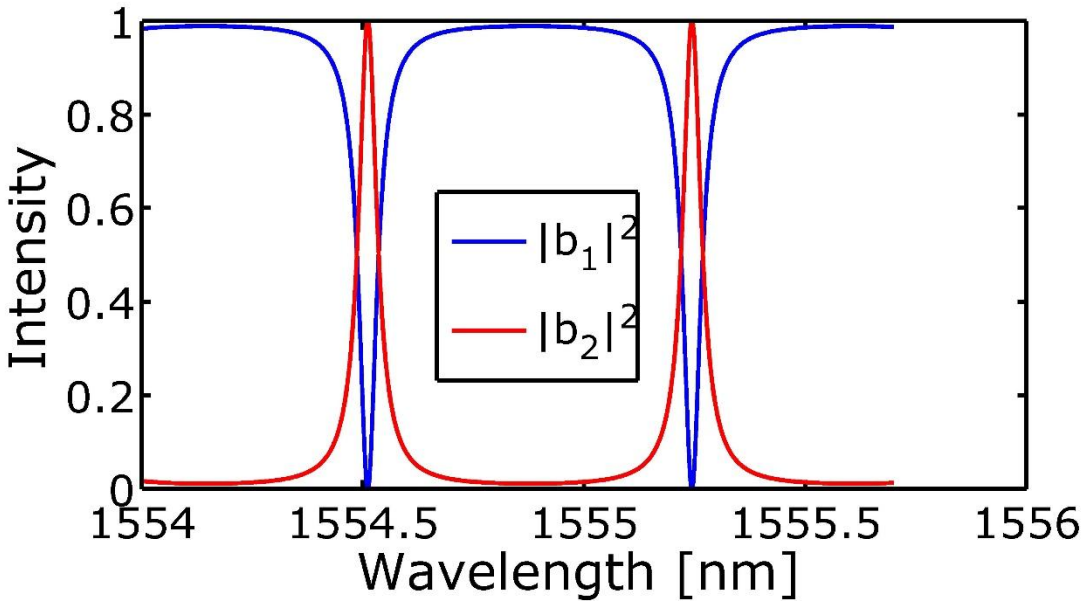

Figure 3.4. Resonances of the microring coupled to two waveguides

3.3 Microring resonator parameters.

3.3.1 Free spectral range.

Micro ring resonators can be described using the same parameters used in describing optical cavities. The distance between two resonance peaks is called free spectral range (FSR). When in resonance $L\beta = 2\pi m,$ where β is the propagation constant $\beta = k_0 n_{eff}$, here $k_0 = 2\pi/\lambda$ and *L*, $(L = 2\pi R)$ is the perimeter of the ring. One way of approximating the FSR (in the wavelength domain) using the propagation constant is, neglecting the wavelength dependence of the effective refractive index,

$$\frac{\partial\beta}{\partial\lambda} = \left(\frac{\partial}{\partial\lambda}\frac{2\pi}{\lambda}\right) neff + k_0 \frac{\partial}{\partial\lambda} n_{eff},$$

$$\frac{\partial\beta}{\partial\lambda} \approx -\frac{1}{\lambda}\frac{2\pi}{\lambda} n_{eff},$$

$$\frac{\partial\beta}{\partial\lambda} \approx -\frac{\beta}{\lambda}. \tag{3.28}$$

The FSR is of the form:

$$FSR = \Delta\lambda = \frac{\Delta\beta}{\partial\beta/\partial\lambda} = \frac{-2\pi/L}{-\beta/\lambda} = \frac{-2\pi/L}{-k_0 n_{eff}/\lambda} \approx \frac{\lambda^2}{L n_{eff}}. \tag{3.29}$$

If the wavelength dependence of the effective refractive index cannot be neglected a modified form of the FSR can be obtained as:

$$\frac{\partial\beta}{\partial\lambda} = -\frac{1}{\lambda} k_0 n_{eff} + k_0 \frac{\partial}{\partial\lambda} n_{eff},$$

$$\frac{\partial\beta}{\partial\lambda} = -\frac{1}{\lambda} k_0 n_g,$$

where the group index is defined as follow:

$$n_g = n_{eff} - \lambda \frac{\partial}{\partial\lambda} n_{eff}. \tag{3.30}$$

The group index can be used instead of the effective index to obtain more accurate values of the FSR. Then the modified value of the FSR is then given by,

$$FSR = \frac{\lambda^2}{Ln_g}. \tag{3.31}$$

The FSR is a quantity inversely proportional to the perimeter of the ring, so in applications where a greater spectral range is required a smaller radius would be useful.

3.3.2 Full Width at Half Maximum

Another important parameter to know is the width of the resonance peak defined as the full width at hall maximum (FWHM). From Equation (3.10) and (3.12) we have:

$$\frac{\alpha^2\left(1-|\tau|^2\right)}{1+\alpha^2|\tau|^2-2\alpha|\tau|\cos\left(\phi+\varphi_\tau\right)} = \frac{1}{2}\frac{\alpha^2\left(1-|\tau|^2\right)}{\left(1-\alpha|\tau|\right)^2},$$

without considering the phase term we obtain,

$$1+\alpha^2|\tau|^2-2\alpha|\tau|\cos\left(\phi\right) = 2\left(1-\alpha|\tau|\right)^2. \tag{3.32}$$

For small ϕ the series expansion of the Euler formula can be used, so:

$$\cos\phi = 1-\frac{\phi^2}{2}, \tag{3.33}$$

therefore;

$$-2\alpha|\tau|\left(1-\frac{\phi^2}{2}\right) = 2\left(1-\alpha|\tau|\right)^2-\alpha^2|t|^2-1,$$

$$\phi^2 = \frac{2\left(1-\alpha|\tau|\right)^2-\alpha^2|\tau|^2-1+2\alpha|\tau|}{\alpha|\tau|},$$

$$\phi^2 = \frac{2\left(1-\alpha|\tau|\right)^2-\left(1-\alpha|\tau|\right)^2}{\alpha|\tau|},$$

$$\phi = \frac{1-\alpha|\tau|}{\sqrt{\alpha|\tau|}}. \tag{3.34}$$

In the wavelength domain compared to the phase change of 2π for the FSR we have:

$$\frac{FWHM}{FSR} = \frac{2\phi}{2\pi},$$

$$FWHM = \frac{2\phi}{2\pi} FSR,$$

$$FWHM = \frac{2\left(1-\alpha|\tau|\right)}{2\pi\sqrt{\alpha|\tau|}} \frac{\lambda^2}{Ln_g}. \tag{3.35}$$

Assuming a weak coupling, that is $\kappa \ll 1$, and $\alpha = |\tau| \approx 1$ we have the expression:

$$FWHM = \frac{\kappa^2 \lambda^2}{\pi Ln_g}. \tag{3.36}$$

3.3.3 *Finesse*

Another important parameter describing a resonator is the finesse that is defined its free spectral range divided by the bandwidth (FWHM) of its resonances. From the previous results we obtain the finesse of the micro ring resonator as:

$$F = \frac{FSR}{FWHM} = \frac{\lambda^2 / Ln_g}{\kappa^2 \lambda^2 / \pi Ln_g} = \frac{\pi}{\kappa^2}, \tag{3.37}$$

it is determined by the resonator losses and is independent of the ring length.

3.3.4 *Q Factor*

A resonator Q factor is a parameter that characterizes the bandwidth of a resonator relative to its center frequency. A large Q indicates a slow rate of energy loss relative to the stored energy in the resonator. There can be two definitions of the Q factor that are not necessary the same, they become equivalent as the Q factor becomes larger. The first definition is:

$$Q = 2\pi \times \frac{\text{Stored energy per cycle}}{\text{Lost energy per cycle}}, \tag{3.38}$$

the 2π factor is keep to maintain the equivalence with the other definition at high Q.

The other definition is the ratio of the center frequency relative to the bandwidth of a resonance.

$$Q = \frac{\lambda}{FWHM} = \frac{\pi L n_g}{\kappa^2 \lambda} = F \frac{L n_g}{\lambda} \tag{3.39}$$

The Q factor is directly proportional to the ring perimeter, the Q factor rises as the ring perimeter is increased, because this decrease the optical loss per cycle. However, high Q values can be achieved not only by using very long resonators, but rather by strongly reducing the losses per round trip. The Q factor of a resonator is a measure of the sharpness of the resonance, high-Q resonators can be used for obtaining laser output with a very narrow linewidth

3.4 The transfer matrix.

The transfer matrix method is a method used to analyze the propagation of electromagnetic waves through a stratified medium. In this section we use this method to obtain the transfer matrix of a micro ring resonator coupled to an optical waveguide. From the matrix in Equation (3.1)

$$\begin{pmatrix} b_1 \\ b_1' \end{pmatrix} = \begin{pmatrix} \tau & \kappa \\ -\kappa^* & \tau^* \end{pmatrix} \begin{pmatrix} a_1 \\ a_1' \end{pmatrix},$$
$$\begin{pmatrix} b_1 \\ b_1' \end{pmatrix} = \mathbf{M} \begin{pmatrix} a_1 \\ a_1' \end{pmatrix}. \tag{3.40}$$

The $\mathbf{M}$ matrix relates linearly the two output mode amplitudes (b_1, b_1') and the two input mode amplitudes (a_1, a_1') with the coupler through the coupling parameters (τ, κ). Using Equation (3.4) and (3.5)

$$b_1 = \tau a_1 + \kappa a_1', \tag{3.4}$$

$$b_1' = -\kappa^* a_1 + \tau^* a_1', \tag{3.5}$$

dividing Equation (3.5) by κ^* and solving for a_1 we arrive to,

$$\frac{b_1'}{\kappa^*} = -a_1 + \frac{\tau^*}{\kappa^*} a_1',$$

$$a_1 = \frac{\tau^*}{\kappa^*} a_1' - \frac{1}{\kappa^*} b_2, \tag{3.41}$$

substituting Equation (3.41) in Equation (3.4) we obtain:

$$b_1 = \tau\left(\frac{\tau^*}{\kappa^*} a_1' - \frac{1}{\kappa} b_1'\right) + \kappa a_1',$$

$$b_1 = -\frac{\tau}{\kappa^*} b_1' + \left(\frac{|\tau|^2}{\kappa^*} + \kappa\right) a_1',$$

$$b_1 = -\frac{\tau}{\kappa^*} b_1' + \left(\frac{|\tau|^2 + |\kappa|^2}{\kappa^*}\right) a_1',$$

with Equation (3.2) de arrive to:

$$b_1 = \frac{1}{\kappa^*} a_1' - \frac{\tau}{\kappa^*} b_1', \tag{3.42}$$

rewriting Equation (3.41) and Equation (3.42) in a matrix form,

$$\begin{pmatrix} a_1 \\ b_1 \end{pmatrix} = \frac{1}{\kappa^*}\begin{pmatrix} \tau^* & -1 \\ 1 & -t \end{pmatrix}\begin{pmatrix} a_1' \\ b_1' \end{pmatrix} = \mathbf{T}\begin{pmatrix} a_1' \\ b_1' \end{pmatrix}. \tag{3.42}$$

The matrix $\mathbf{T}$ is a linear relationship between the two mode amplitudes of one waveguide to the mode amplitudes of the ring. This matrix is regarded as the system's transfer matrix.

We have studied two geometries of a microring resonator-waveguide system. The geometry with two waveguides is the analog of the Fabry Perot cavity used in the previous chapter and is the basis to describe the coherent microring perfect absorber.

4 DESIGN AND FABRICATION PROCESS

We have studied a device that can fully extinguish the outgoing radiation, such a device can be formed with a slab of thickness d and complex refractive index. Now, we show that a microring resonator coupled to two optical waveguides can act as a coherent perfect absorber if the right conditions are satisfied. We design, fabricate, and characterized a device with this geometry.

4.1 The Coherent microring perfect absorber model

Years ago fully absorption of light into a microring resonator was demonstrated [28] using an optical fiber to couple light into the cavity. This fully absorption phenomenon was termed as "critical coupling". Although this device can be regarded as a one channel CPA we cannot control the spatial distribution of the input field. In a recent work [3], the enhance and suppression of absorption was demonstrated using a silicon slab i.e. a two channel CPA. Illuminating a cavity with two beams of equal amplitude traveling in opposite direction and changing its relative phase difference one can enhance or suppress the absorption. With this phase control device is possible to turn absorption almost completely on or off. Hence the CPA could work as an optical switch, optical modulator, or optical detector and could see potential applications in silicon photonic devices.

A model of the proposed device is presented in Figure 4.1 As we studied in the previous chapter, using the coupled mode theory wen can relate the input and output fields by the coupling matrix, the fields amplitudes in the first coupler are related by the matrix:

$$\begin{pmatrix} b_1 \\ b_1' \end{pmatrix} = \begin{pmatrix} \tau_1 & \kappa_1 \\ -\kappa_1^* & \tau_1^* \end{pmatrix} \begin{pmatrix} a_1 \\ a_1' \end{pmatrix}, \tag{4.1}$$

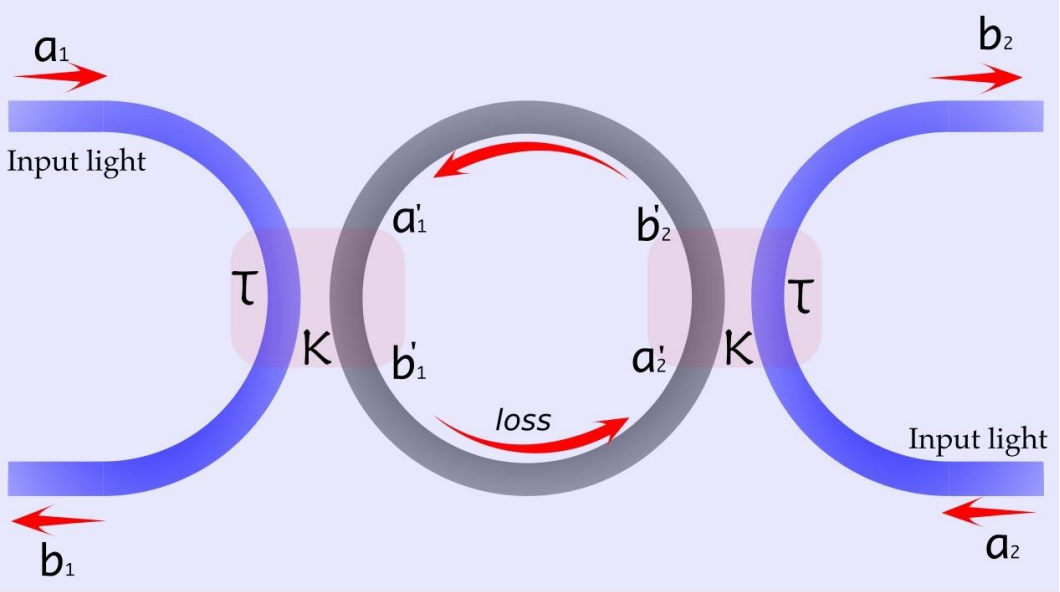

Figure 4.1. Schematic model of the proposed CPA with a lossy micro ring resonator of a 50 μm radius, input and output wave intensities are marked with arrows. The letter κ represents the coupling strength between the mode in the waveguide and the mode in the microring. The separation between the waveguide and the microring is 150 nm

and the fields in the second coupler are related by the matrix,

$$\begin{pmatrix} b_2 \\ b_2' \end{pmatrix} = \begin{pmatrix} \tau_2 & -\kappa_2^* \\ \kappa_2 & \tau_2^* \end{pmatrix} \begin{pmatrix} a_2 \\ a_2' \end{pmatrix}, \tag{4.2}$$

where (a_1', a_2', b_1', b_2') are the field amplitudes at the input/output of each coupler in the ring resonator and are related by the matrix

$$\begin{pmatrix} b_2' \\ a_2' \end{pmatrix} = \begin{pmatrix} e^{-iknL/2} & 0 \\ 0 & e^{iknL/2} \end{pmatrix} \begin{pmatrix} a_1' \\ b_1' \end{pmatrix}. \tag{4.3}$$

This matrix is regarded as the propagation matrix. Here e^{iknL} is the total accumulated phase when a wave travels around the ring, L is the length of the ring, n is the refractive index and is of the form $n = n_r + in_i$, for gain $ni < 0$ and for loss $n_i > 0$.

Using the matrices in Equation (4.1) and (4.2) we can obtain the transfer matrix linearly relating the fields in the waveguide with the fields in the microring

$$\begin{pmatrix} a_1' \\ b_1' \end{pmatrix} = \frac{1}{\kappa_1}\begin{pmatrix} -\tau_1 & 1 \\ -1 & \tau_1^* \end{pmatrix}\begin{pmatrix} a_1 \\ b_1 \end{pmatrix}, \tag{4.4}$$

$$\begin{pmatrix} b_2 \\ a_2 \end{pmatrix} = \frac{1}{\kappa_2}\begin{pmatrix} \tau_2 & -1 \\ 1 & -\tau_2^* \end{pmatrix}\begin{pmatrix} b_2' \\ a_2' \end{pmatrix}, \tag{4.5}$$

and with Equation (4.3), (4.4), and (4.5) we obtain the relationship

$$\begin{pmatrix} b_2 \\ a_2 \end{pmatrix} = \frac{1}{\kappa_2}\begin{pmatrix} \tau_2 & -1 \\ 1 & -\tau_2^* \end{pmatrix}\begin{pmatrix} e^{-iknL/2} & 0 \\ 0 & e^{iknL/2} \end{pmatrix}\frac{1}{\kappa_1}\begin{pmatrix} -\tau_1 & 1 \\ -1 & \tau_1^* \end{pmatrix}\begin{pmatrix} a_1 \\ b_1 \end{pmatrix}. \tag{4.6}$$

In this analysis we assume symmetric coupling $\left(\text{i.e. } \tau_1 = \tau_2 = \tau, \kappa_1 = \kappa_2 = \kappa\right)$. Here we are going to use the expressions obtained in the appendix A for the coupling parameters:

$$\begin{aligned} \tau &= \cos\theta \\ \kappa &= i\sin\theta \end{aligned} \tag{4.7}$$

where $\theta = |\kappa| l_{\text{coupler}}$ is defined as the coupling angle in the coupling areas $|\kappa|$ is the coupling constant and l_{coupler} is the coupler length. Substituting Equation (4.7) in Equation (4.6) we obtain:

$$\begin{aligned} \begin{pmatrix} b_2 \\ a_2 \end{pmatrix} = \frac{1}{i\sin\theta}\begin{pmatrix} \cos\theta & -1 \\ 1 & -\cos\theta \end{pmatrix} \times \begin{pmatrix} e^{-iknL/2} & 0 \\ 0 & e^{iknL/2} \end{pmatrix} \times \\ \frac{1}{i\sin\theta}\begin{pmatrix} -\cos\theta & 1 \\ -1 & \cos\theta \end{pmatrix} \times \begin{pmatrix} a_1 \\ b_1 \end{pmatrix}. \end{aligned} \tag{4.8}$$

The first step is to obtain the conditions for fully absorption, considering the case of resonance $\left(n_r kL = \phi = 2m\pi\right)$ we have:

$$\begin{pmatrix} b_2 \\ a_2 \end{pmatrix} = \frac{1}{\sin^2\theta}\begin{pmatrix} e^{\gamma/2}\cos^2\theta - e^{-\gamma/2} & -2\sinh\left(\frac{\gamma}{2}\right)\cos\theta \\ 2\sinh\left(\frac{\gamma}{2}\right)\cos\theta & e^{-\gamma/2}\cos^2\theta - e^{\gamma/2} \end{pmatrix}\begin{pmatrix} a_1 \\ b_1 \end{pmatrix}. \tag{4.9}$$

.

Here we have defined $\gamma = kn_i L$ as the distributed loss coefficient. The conditions for perfect absorbing the incident waves is to have zero reflections, so these conditions are:

$$\begin{aligned} &a_1, a_2 \rightarrow \text{finite}, \\ &b_1 = b_2 = 0, \end{aligned} \tag{4.10}$$

therefore the transfer matrix elements must satisfy:

$$T_{11} = 0 \text{ and } a_2 = T_{21} a_1, \tag{4.11}$$

from the last conditions we obtain the relationship,

$$e^{\gamma/2} \cos^2\theta - e^{-\gamma/2} = 0,$$

$$e^{\gamma/2} \cos^2\theta = e^{-\gamma/2},$$

$$\cos^2\theta = \frac{e^{-\gamma/2}}{e^{\gamma/2}} = e^{-\gamma},$$

$$\boxed{\cos\theta = e^{-\gamma/2}}. \tag{4.12}$$

We realize that Equation 4.12 is exactly the critical coupling condition (coupling parameter is equal to the internal loss) and is exclusively determined by the device and is independent of the initial conditions. In addition, the previous condition shows that the initial conditions must satisfy $a_1 = a_2$ to have perfect absorption what implies $T_{21} = 1$, under this conditions the transfer matrix reduces to:

$$\begin{pmatrix} b_2 \\ a_2 \end{pmatrix} = \begin{pmatrix} 0 & -1 \\ 1 & e^{-\gamma/2} e^{-\gamma} - e^{\gamma/2} \end{pmatrix} \begin{pmatrix} a_1 \\ b_1 \end{pmatrix}. \tag{4.13}$$

So far, we have derived the conditions for perfect absorption: the coupling losses $\cos\theta$ must be equal to the half trip internal losses $\exp(-\gamma/2)$ and the input waves must have the same amplitude and phase.

Perfect absorption occurs when an interference trap is created into the cavity, in this way, input waves with a specific spatial pattern are

trapped and eventually get absorbed by the lossy medium. For this device, in the critical coupling condition the absorption is strongly enhanced. So, for having strong absorption we need a critically coupled microring, two input waves with the correct phase and equal amplitude.

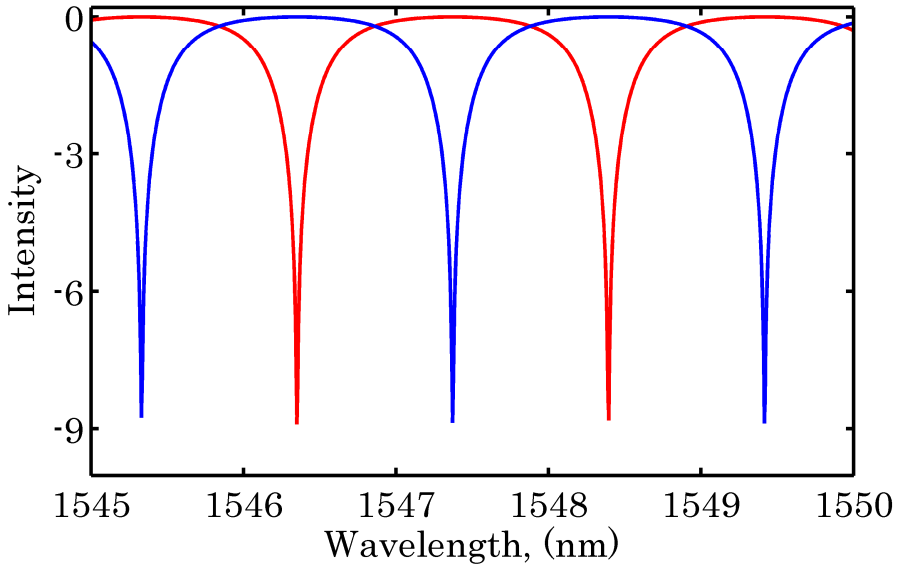

Figure 4.2. Semilog plot of the CPA resonances when the condition of Equation 4.12 is satisfied. When the critical coupling condition is achieved the absorption is increased up to nine orders of magnitude. Red (blue) line is the output intensity when the input waves have zero (π) phase difference

From Equation (4.8), we obtain the matrix which relates the input and output waves in the form:

$$\begin{pmatrix} b_1 \\ b_2 \end{pmatrix} = \frac{1-|\tau|^2}{|\tau|^2 e^{+ikna} - e^{-ikna}} \begin{pmatrix} \dfrac{|\tau| 2i \sin(kna)}{1-|\tau|^2} & 1 \\ 1 & \dfrac{|\tau| 2i \sin(kna)}{1-|\tau|^2} \end{pmatrix} \begin{pmatrix} a_1 \\ a_2 \end{pmatrix}. \qquad (4.14)$$

We also found that the relative phase difference must be $n\pi$ for perfect absorption. Input waves with different phase difference will not be fully absorbed, because the interference trap is not created and eventually they escape.

Figure 4.2 shows a Semilog plot of the CPA resonances when the input phase difference is 0 (red) and π (blue), the simulated device has a 50 μm radius. Red line corresponds to $|b_1|^2$ and $|b_2|^2$ when the input phase is 0, blue line corresponds to a phase difference of π. In this case we are in the critical coupling condition, achieving an absorption up to nine orders of magnitude.

Figure 4.3 is a COMSOL simulation of the device when the perfect absorption conditions are satisfied. The integrated ring resonator has a high index contrast. The black arrows show the input waves, the output waves are represented by the red arrows, as we see there is no output waves meaning that the light is fully absorbed in the ring resonator

To fully understand the properties of the CPA we consider the effects of changing the relative phase between the input waves. If we suppose two normalized input waves of equal intensities of the form $[1, \pm\exp(j\varphi)]/\sqrt{2}$. Changing the relative phase difference we can enhance or suppress the absorption.

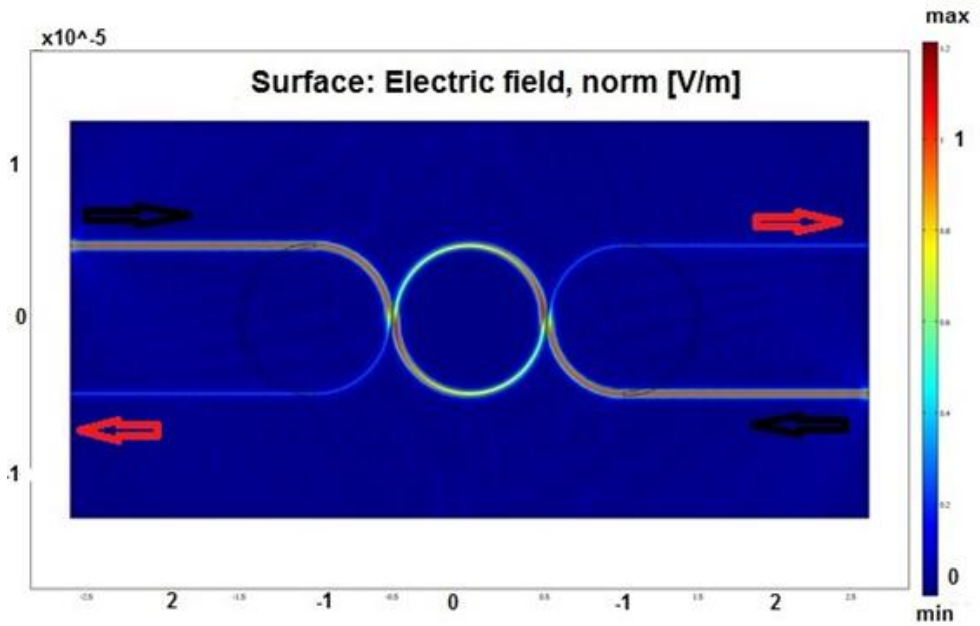

Figure 4.3. Simulation of a CPA with a high index contrast microring resonator.

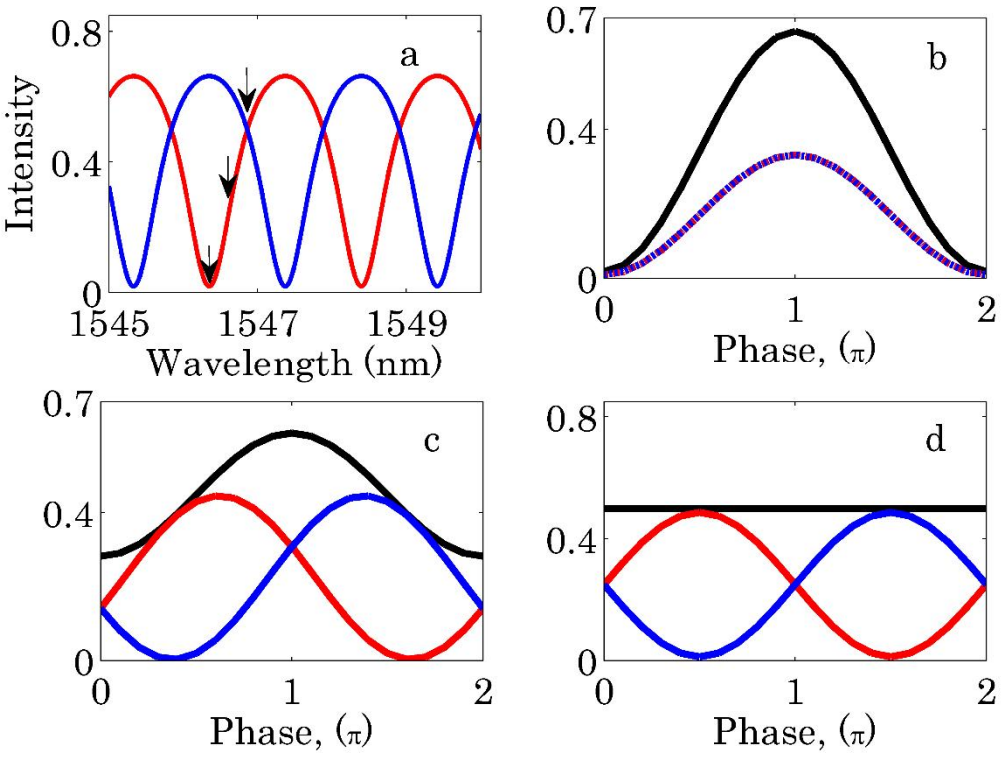

Figure 4.4 a) Normalized total output intensity $|b_1|^2 + |b_2|^2$ as function of the wavelength when the input waves have a zero (red) and π (blue) phase difference. Arrows point to three wavelengths of interest (1546.35, 1546.6, and 1546.86). b-d) Individual output intensities for each channel $|b_2|^2$ (blue) $|b_1|^2$ (red) for the marked wavelengths as the phase difference is varied from 0 to π . Black line represents the total output intensity $|b_1|^2 + |b_2|^2$ as the phase is varied. The point where blue and red lines crosses in a) is a phase insensitive wavelength, as we observe in d), the total output intensity is constant for each phase.

Figure 4.4 shows the total normalized output intensities from the left and right waveguides as a function of the wavelength. The CPA resonances are parity odd (4.4 a) red) and parity even (4.4 a) blue). When the input phase is between 0 and π the output intensities do not correspond to CPA modes. This characteristic of the CPA enable us tuning the absorption from zero to full absorption by changing the relative phase difference between the input waves. This property makes the CPA useful for switching applications.

4.2 *Design of the coherent perfect absorber.*

Waveguides for integrated photonics devices serve as transmission media. Due to the easy fabrication waveguides with rectangular cross section are usually used. The CPA device was designed based on silicon waveguide embedded in SiO_2 rectangular cross section of $450\text{nm} \times 220\text{nm}.$ This dimension was used in other photonics devices [30, 31, 32]. The asymmetric dimension of this kind of waveguides have different optical properties when transmitting light with different polarizations. In this work the waves with electric field polarized in the plane of the chip are referred as TE polarized. This waveguide is single mode at the proposed working wavelength of $\sim 1.55\mu\text{m}$. The dimensions of the waveguide ensure a maximal confinement of light in the core.

Bending the straight waveguide we obtain a microring resonator which FSR is inversely proportional to the ring radius according to Equation (3.31) in the previous chapter. For achieving higher FSR a smaller radius is needed. However as the radius get smaller the bending loss get significant which limit the quality factor. In this design, a $50\mu\text{m}$ radius microring where the bending loss can be negligible [33].

A high Q is usually desired for a resonator. The operating Q depends inversely on the coupling efficiency κ^2 according to Equation (3.39). The straightforward way of tuning the coupling efficiency is to adjust the gap (distance) between the input waveguide and the microring. For this device a separation distance of 150nm was used. With this distance a Q factor of about ~4000 is achieved. The 150nm gap size can be well controlled with electron beam lithography, which makes the device practical at the fabrication stage.

The optical design of the CPA is shown in Figure 4.5. The size of the chip is about 4mm in length and 4mm in width. This size is the minimal capable of being manipulated comfortably with tweezers. The input and output ports both ends are with nanotapers [33], which make characterization convenient. Nanotapers are used to reduce insertion loss and to greatly increase the fiber to waveguide coupling efficiency. In order to achieve equal intensity at the couplers the input waveguide

is designed in a "Y" branch shape. For the device shown in Figure 4.5 the arm's length is the same for both, $(\sim 1300\mu\mathrm{m})$ the right and left arm. With this design we ensure equal waves intensities and equal phase relationship at the coupling region. In order to change the phase of one of the input waves the arm length was modified slightly. In this work two devices were fabricated, one with equal arm length and the other with an arm length difference of $150\mu\mathrm{m}$, the choice of this length difference is suitable for observe the effect of the phase difference in the CPA.

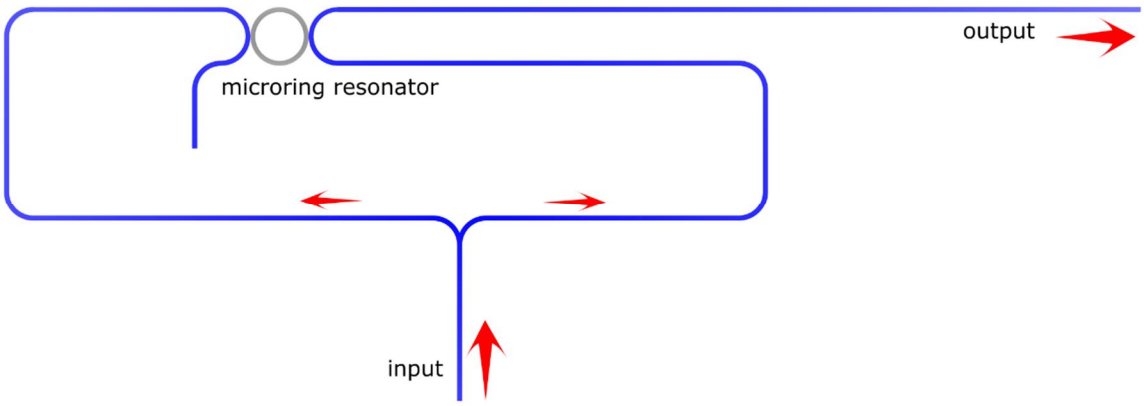

Figure 4.5. Optical design of the CPA, The input waveguide is designed in a Y branch shape. Input waves are marked with arrows. Output wave is marked with a red arrow at the right side.

4.3 *Fabrication process flow.*

4.3.1 *Electron-beam Lithography*

Electron-beam lithography often called e-beam lithography is the practice of scanning a focused beam of electrons to draw custom patterns on a surface covered with an electron-sensitive film called resist. The e-beam changes the solubility of the resist enabling selective removing of either exposed or non-exposed area of the resist depending on the resist type. The purpose is to create very small structures in the resist that can subsequently be transferred to the substrate material, often by etching. Compared to photolithography, e-beam lithography

can create smaller structures in the resist because it beats the diffraction limit of light. It can draw custom patterns with sub-10 nm resolution. The key limitation of ebeam lithography is throughput. A very long exposure time is often needed for a common sample. The high resolution and low throughput limit its usage to photomask fabrication, low volume production of semiconductor devices, research and development.

The patterning of our device based on 450 nm width waveguide with nanometer precision is beyond the capabilities of the conventional photolithography systems, we decided to use ebeam lithography for the device patterning. The Leica EPBG 5000+ system for patterning the optical layer of the designed device is an advanced ebeam lithography system capable of reproducibly achieving feature sizes less than 10nm.

The EPBG system can align different patterns. Alignment marks are always needed on the pre-existing pattern. The EPBG can establish a coordinate system based on alignment marks detected on the wafer and precisely place a pattern with respect to pre-existing patterns.

4.3.2 Fabrication

Using the design described in the previous section, the CPA device was fabricated. The fabrication is totally compatible with silicon-on-insulator (SOI) technology, which makes the device very promising for photonic integrated circuits.

The fabrication process flow is shown in Figure 4.6. The fabrication started with a SOI wafer with 220 nm thick Si device layer over a 2μm buried oxide layer. The layer thickness was chosen according to the

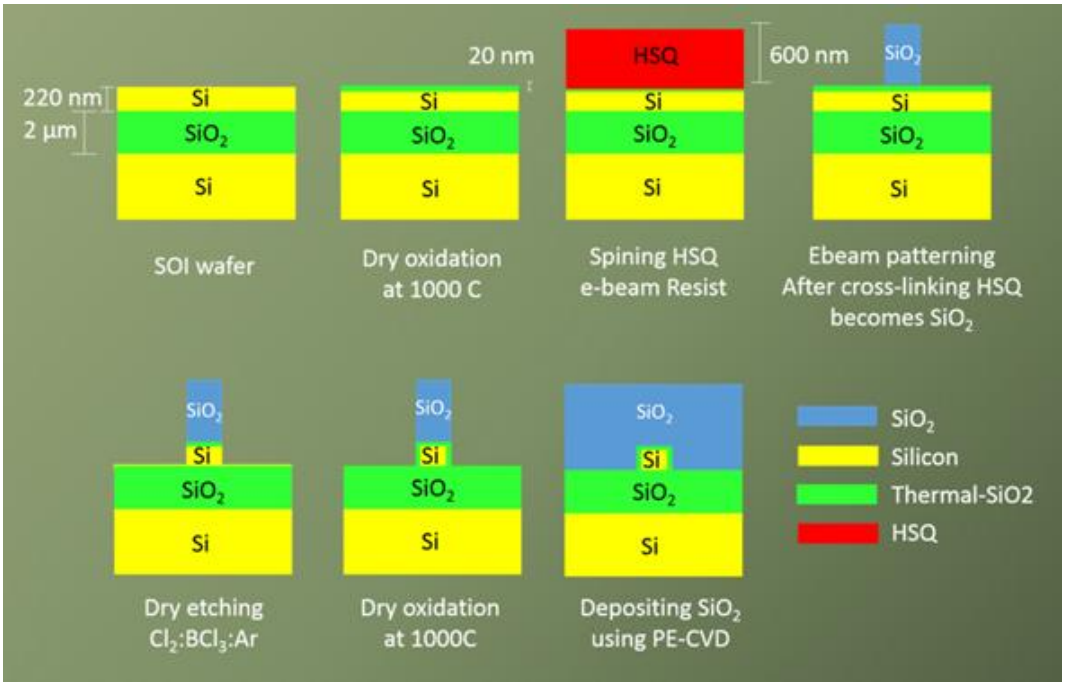

Figure 4.6. Fabrication process flow. (Figure extracted from reference **[35]**)

designed waveguide dimension. The waveguide pattern was generated by a Leica EPBG 5000+ ebeam lithography system at 1 nA exposure current with 1 nm beam step. A negative ebeam resist named hydrogen silsesquioxane (HSQ) was used. After spinning the resist at 2500 rpm and baking it at 100°C for 2 minutes a ~600 nm HSQ film was created. The used dose to write the waveguide and ring pattern was 1100 $\mu C/cm^2$. Post exposure baking was carried out at 100°C for 2 minutes. After the patterning process the waveguide pattern was transferred to silicon by Cl_2 dry etching. The dry etching process etched the unpatterned area, leaving a vertical sidewall on the edge of the patterned area, which forms the strip waveguide. The upper SiO_2 cladding was deposited using PE-CVD. Figure 4.7 shows the microring resonator after this process.

The fabricated samples need further processing before they are ready for the characterization process. Integrated photonic circuits

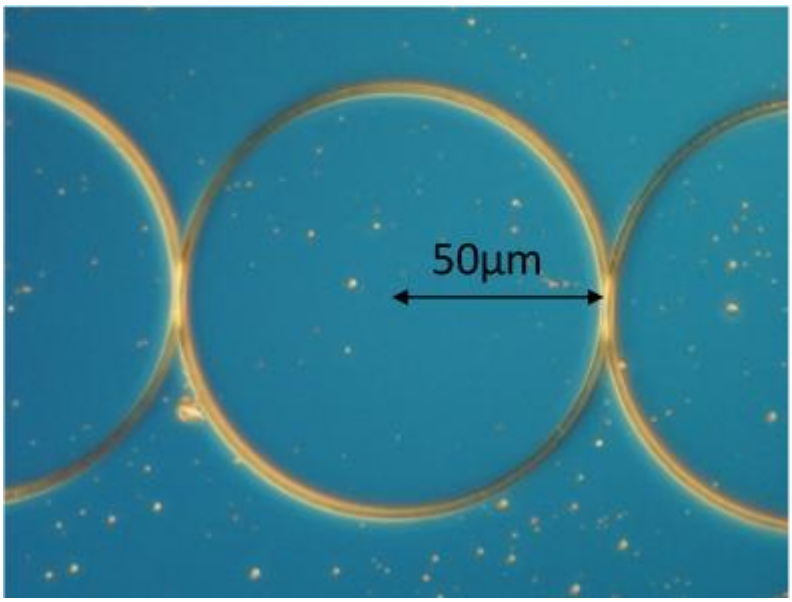

Figure 4.7 Microscope image of the fabricated microring resonator coupled to two optical waveguides.

enable optical devices with multiple functions to be integrated in a very small area of substrate, typical dimensions are from centimeters to even micrometers.

The advantage of the small foot print is to put tens or even hundreds of devices in a single wafer which increase the throughput. Preparation and packing is needed before one can characterize the fabricated device.

4.3.3 Device preparation.

The way the device is tested is to couple light in and out via tapered fiber. This process requires that the input and output waveguides end at the edge of the chip. The facet needs to have a good flatness to avoid big losses due to coupling and scattering. The width of the waveguide was tapered down from 450 nm to 100 nm.

To prepare the sample for optical characterization, the fabricated substrate was diced into small samples. The samples was placed and held in a stable metal surface. Using a vision system and a needle lines are drawn in the x and y direction. Then sample is placed on a sharp

knife and manually is pressed to cut it. The edges after dicing are with roughness on the facets.

Polishing is a common approach to prepare the optical interfaces to obtain ultra-flat and clean facets needed to avoid high light-scattering loss. The nanotaper tips need to be located at the edges of the chip in order to couple light in and out the waveguide efficiently. The samples were polished manually using a rotating plate equipped with diamond lapping films. To manipulate the samples to be polished, the samples were glued on a holder by crystal bond. A lapping film with the larger diamond grit size removes materials faster yielding to a rougher surface. In order to obtain good facet quality and efficiency, the procedure was carried out using a multi-step polishing process. First using a rough lapping film with large diamond grit size, followed by finer films to remove the rough edge left by the last step. The finest film left a very shiny facet. Frequent inspection under microscope is needed in monitoring the polishing process. Over polishing is unacceptable as it will damage the nanotaper. The fabricated device after polishing and ready for the characterization process is shown in Figure 4.8.

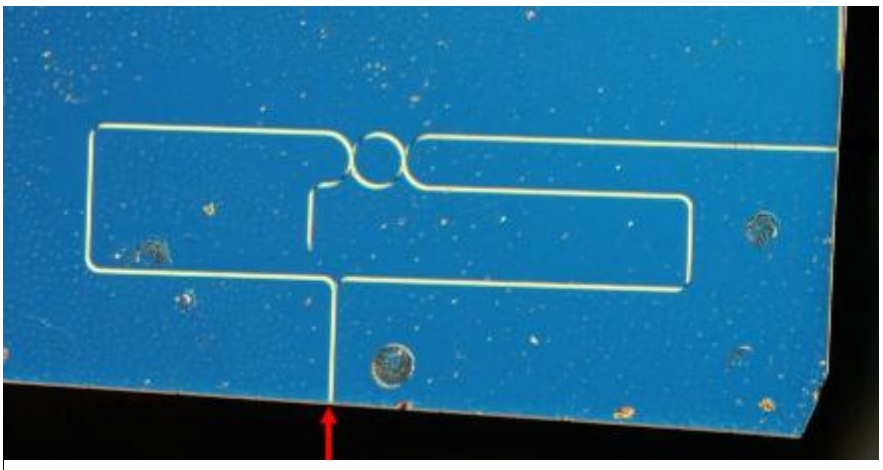

Figure 4.8. Fabricated device after polishing and ready for characterization. Red arrow represents the input. Output waveguide is at the chip right side.

5 DEVICE CHARACTERIZATION

In this chapter the optical method for the characterization process is explained, the measured results are shown and compared with the analytical results obtained in the previous chapter.

5.1 Characterization Setup

The characterization process of the fabricated coherent microring perfect absorber was carried out using our optical setup. The block diagram of the setup is shown in Figure 5-1. In order to characterize the optical properties of the device, light needs to be sent in the input waveguide and collected from the output waveguide. To couple the light into the waveguide a single mode polarization-maintaining tapered fiber was used. To collect the light an objective lens was used instead. A Thor NanoMAX manual XYZ stage with piezo controller was used to align the input tapered fiber to the input waveguide on the sample. The piezo controller and the internal piezos of the stage were used to obtain fine alignment. The fine alignment has 20 nm resolution for all 3 axes and is done without touching the stage. An objective lens was mounted on top of the sample to help monitoring the alignment process. The whole setup was mounted on an optical table with vibration isolation.

The transmitted power was collected using an objective lens. The objective lens makes possible imaging of the output facet of the sample by camera, which gives information of the power distribution at the output. After the objective lens a 4f system was used. Photographs of the setup are shown in Fig 5-2.

We are interested in the spectrum response of the device under test. It can be obtained with our setup, using a tunable laser (0.1 pm resolution) shown in Figure 5-1. A polarizer controller was used in order to have the right light polarization state before it reaches the input waveguide in the chip. Light is then captured with an 20x objective lens. After it, light passes through two 20cm focal length lenses. Once light

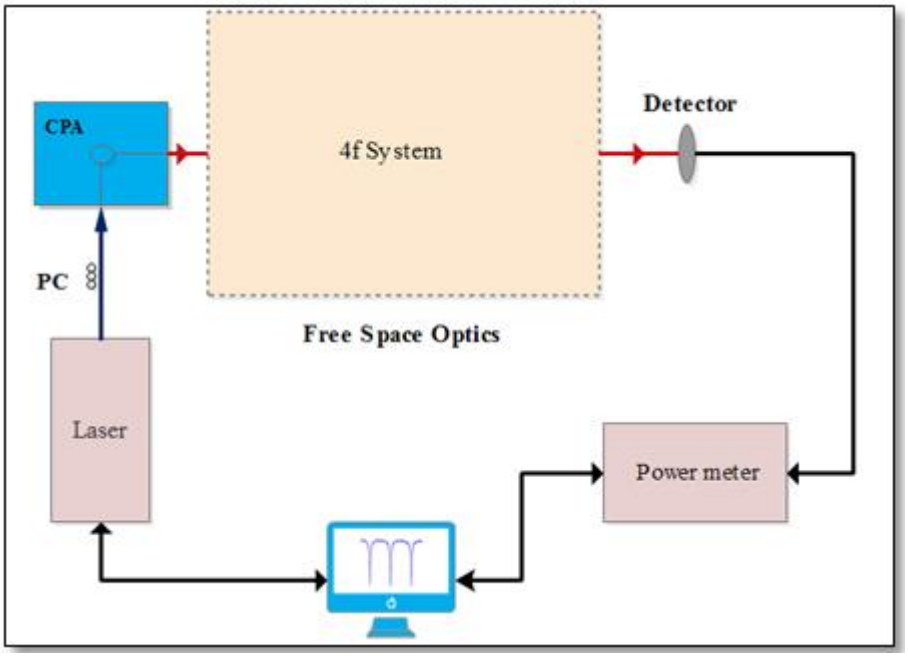

Figure 5.1. Block diagram of the characterization setup.

passes through the second lens it is deviated 90° with a mirror to another lens of 5cm focal length. Then light is captured with an IR camera. The IR camera is helpful to observe the mode profile and to focus the objective lens into the right area at the facet. For measure the output power the mirror is removed and another 20cm focal length lens is collocated and then light reaches the photo detector. A polarizer between the lens and the photo detector was needed on order to measure the right polarization. The optical power was read by a HP optical meter with a resolution of 0.5nW.

While maintaining the output power of the tunable laser, the transmitted optical spectrum response of the device under test was measured by sweeping the output wavelength of the tunable laser and recording the detected transmitted power for each wavelength. Both tunable laser and optical meter were controlled by a computer through GPIB ports. A Matlab program was written to control the tunable laser and the optical meter while recording data.

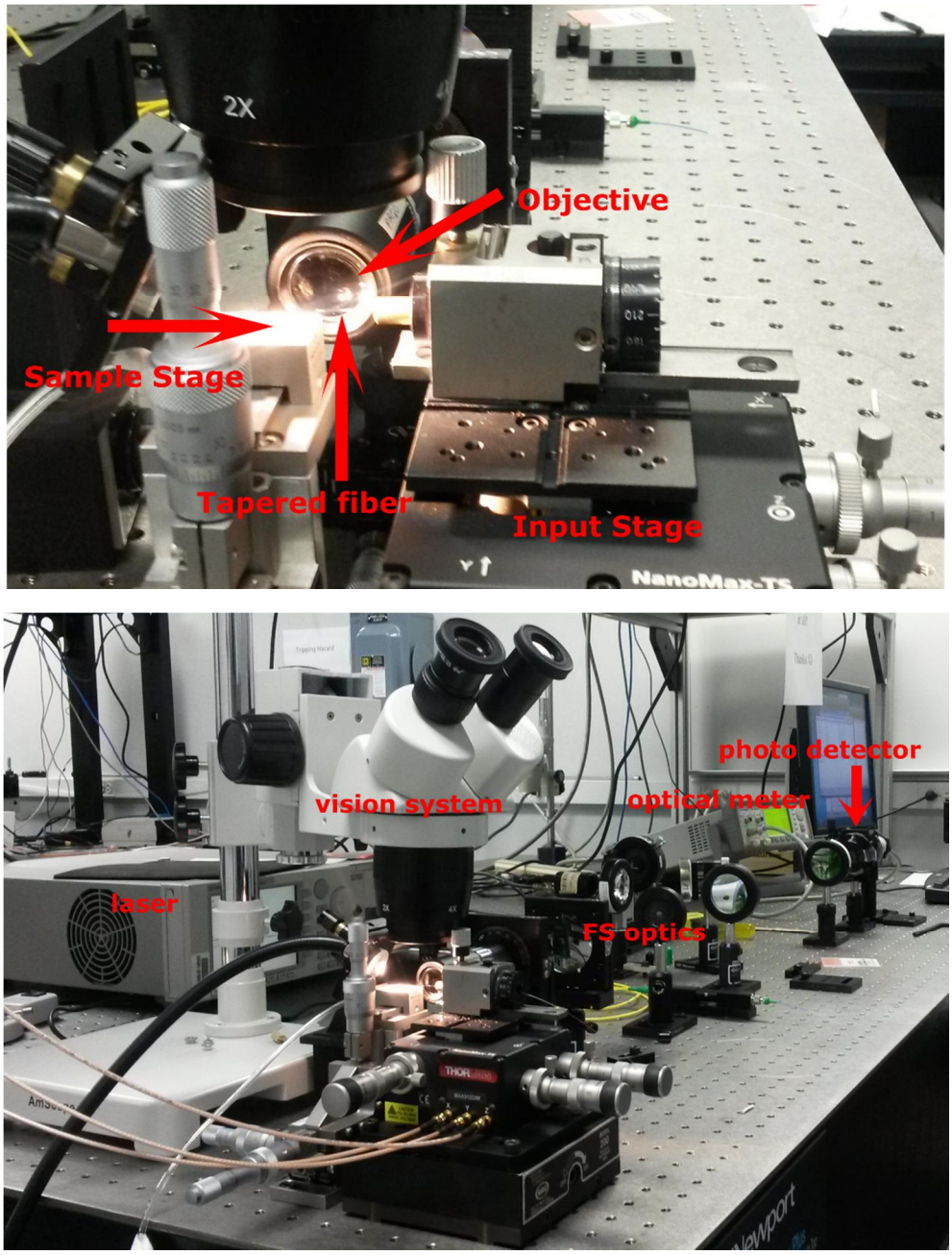

Figure 5.2. Photographs of the characterization setup. Top part, input and sample stage are shown. Bottom part, full setup including the free space optics is shown.

5.2 *Optical spectral response.*

The optical properties of the fabricated CPA were characterized at room temperature. The input polarization was set to TE using the configuration in Figure 5.1. The transmitted power spectra through the output waveguide of the CPA is shown in Figure 5.3 in the wavelength range 1545 nm – 1550 nm.

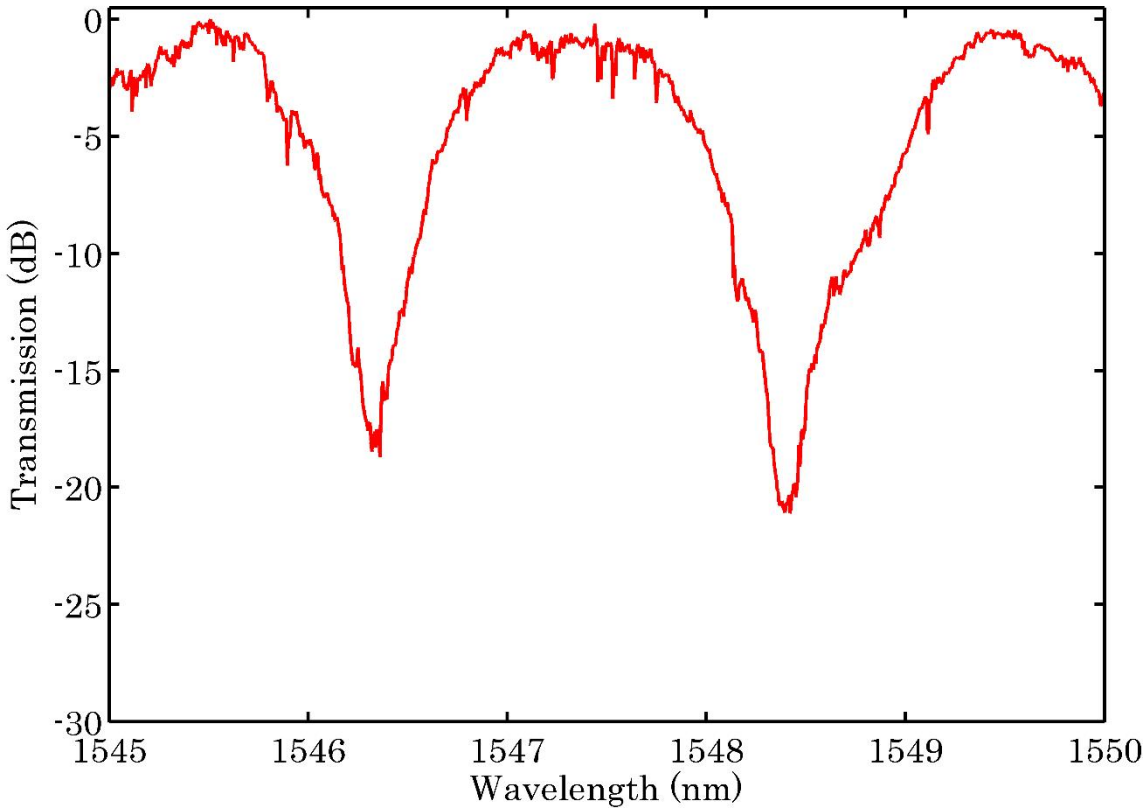

Figure 5.3. Measured transmission spectra of the fabricated coherent microring perfect absorber showing two resonances in the wavelength range.

Each spectrum was normalized to its maximum power. With the data, the values of resonance wavelengths, FSR and FWHM for the TE modes were extracted and listed in Table 5.1.

Table 5.1. Summary of the CPA parameters

Resonance (nm)	1546.35	1548.8
FSR (nm)		2.05
FWHM (nm)	0.375	.475
n_g	3.768	3.723
Q	4118.46	3259.72
F	5.38	4.32

Measurements were repeated for the other CPA with identical design on the same sample. The group index and Q factor for each device were calculated from the extracted parameters using Equations (3.30) and (3.38).

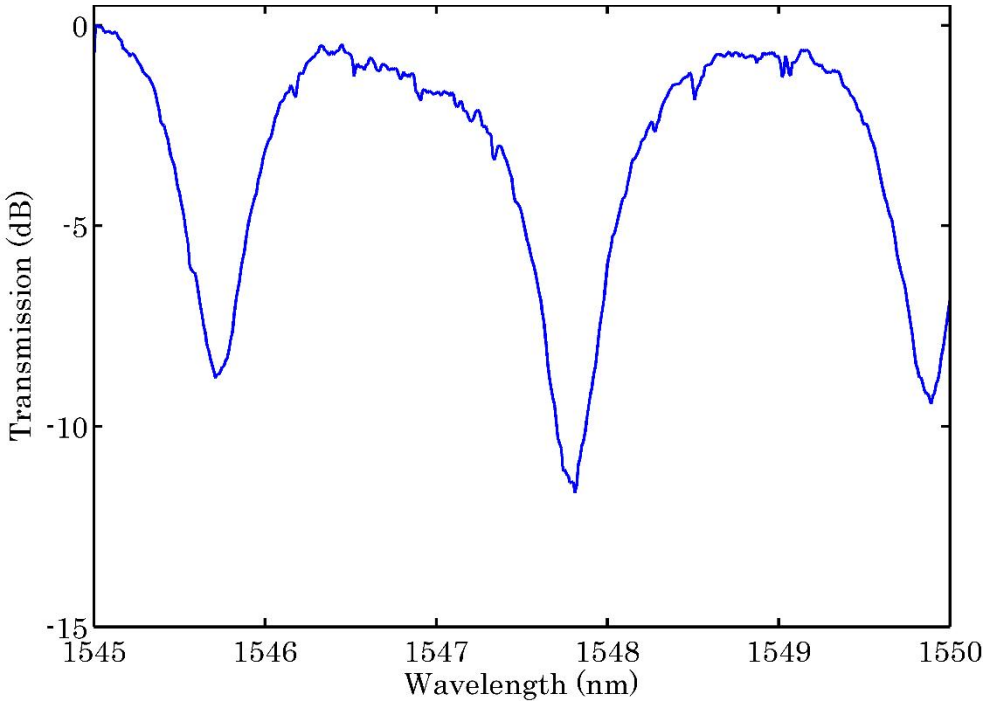

Figure 5.4. Measured transmission spectra of the second fabricated coherent microring perfect absorber showing two resonances in the wavelength range. This device has a 150 μm arm length difference.

The transmitted power spectra through the output waveguide of the CPA with a length arm difference of 150 μm is shown in Figure 5.4

With the data, the values of resonance wavelengths, FSR and FWHM for the TE modes were extracted and listed in Table 5.2.

Table 5.2. Summary of the parameters of the CPA with a phase difference.

Resonance (nm)	1545.71	1547.81	1549.89
FSR (nm)		2.11	2.08
FWHM (nm)	0.4241	.475	.3711
n_g	3.768	3.723	3.676
Q	4118.46	3259.72	4176.50
F	5.38	4.32	5.605

5.3 *Experimental results vs analytical calculations.*

In this section the comparison between the experimental results and the theoretical calculations are presented. For the first CPA, with zero phase difference between the input fields, the results are shown in Figure 5.5.

As we observe the experimental results and the theoretical analysis are in good agreement. For both resonances (1546.35 nm and 1548.4 nm) we have an absorption up to ~23 dB. Figure 5.7 shows the CPA with an arm length difference of 150 μm. As we observe the resonances are shifted to the left. To better observe this effect both results are plotted in Figure 5.6. The shift is about 0.84 nm.

Looking at the resonance of 1546.35 nm, for the CPA with zero phase difference the absorption is about ~23 dB. The arm length

difference almost corresponds to a phase change of about π, so the absorption for the CPA with this phase difference is ~0.5 dB. Absorption at this resonance has been suppressed via phase tuning.

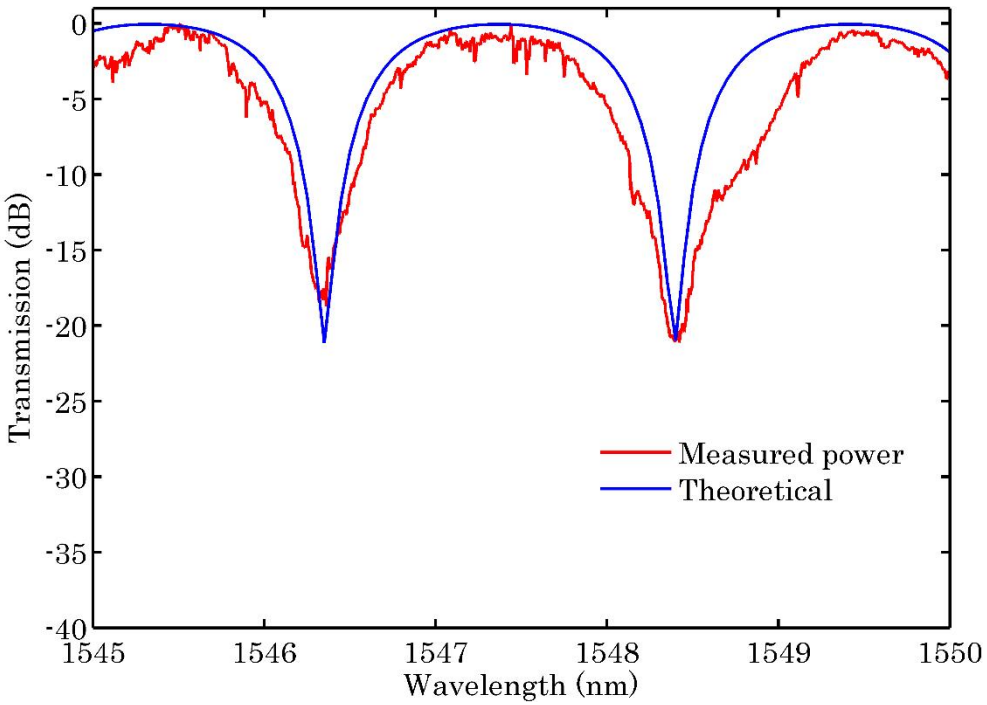

Figure 5.5. Experimental optical response vs analytical data for the CPA with zero phase difference.

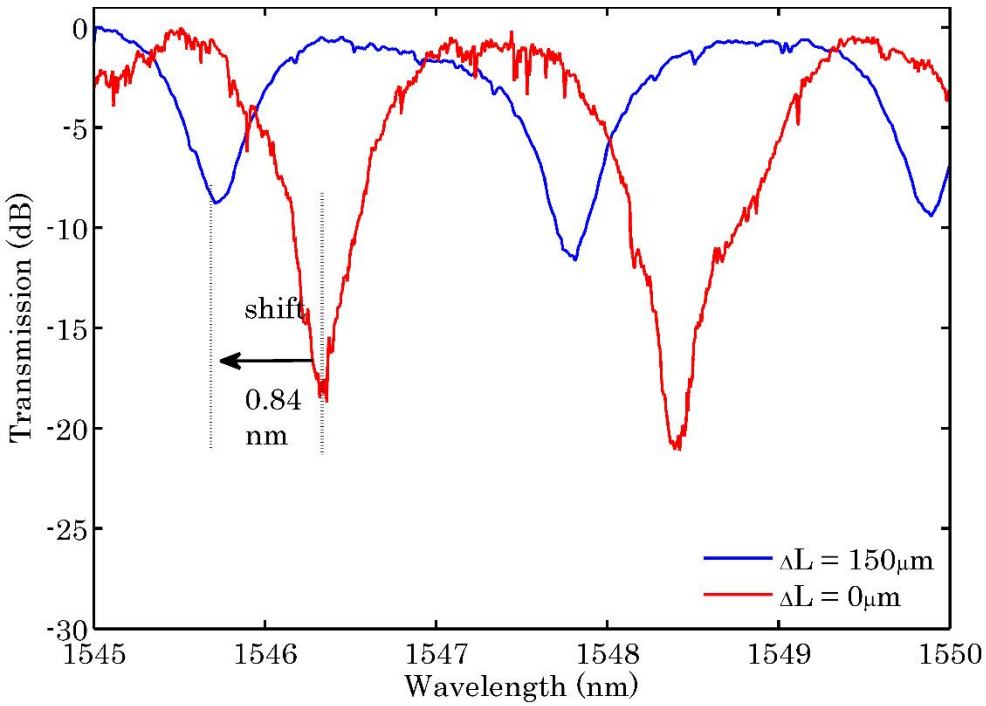

Figure 5.6. Observation of a shift to the left when the arms have a length difference of 150 μm.

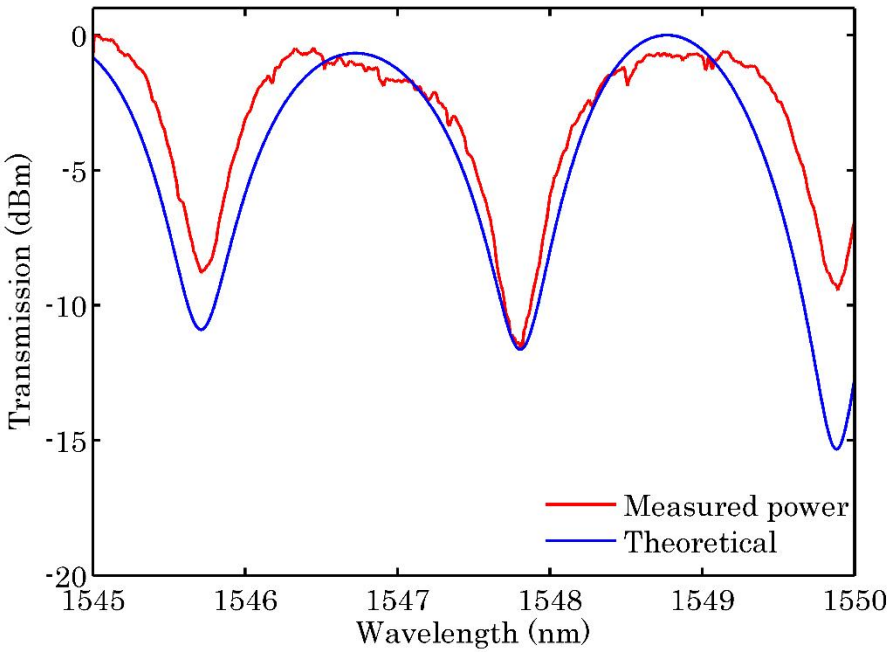

Figure 5.7. Experimental optical response for the CPA with an arm difference of 150μm

Another interesting characteristic of the CPA is that when an input channel is modulated as $e^{i\phi}$, the output intensity will be modulated as:

$$I = I_0 \sin^2(\phi)$$

For appreciate this effect the output power of the CPA 2 (CPA with phase) is plotted in the wavelength range 1540 nm to 1550 nm. The results is shown in Figure 5.8.

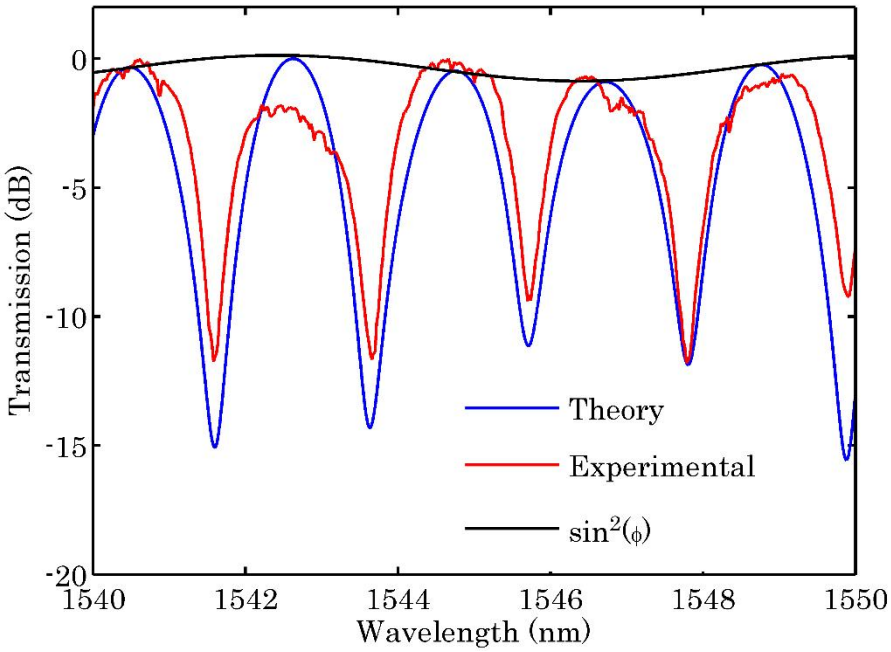

Figure 5.8 Modulated output when there is a phase difference between the input waves.

Normalized output intensity of both CPAs is plotted in Figure 5.9, this intensities almost correspond to those in Figure 4.4 a), the difference is; in Figure 4.4 a) the red line corresponds to the normalized output intensity when the input phase is 0, blue line when the phase is □, in the experimental the blue phase shift introduced by the length difference of 150 μm is almost π .

As we mentioned before, strong absorption occurs at the critical coupling condition, in this case for both CPAs we calculated $\cos\theta / \exp(-\gamma / 2) = 0.6$, in the plot shown in Figure 4.2 this ratio is 1, so, we can say that our device is 60% critically coupled.

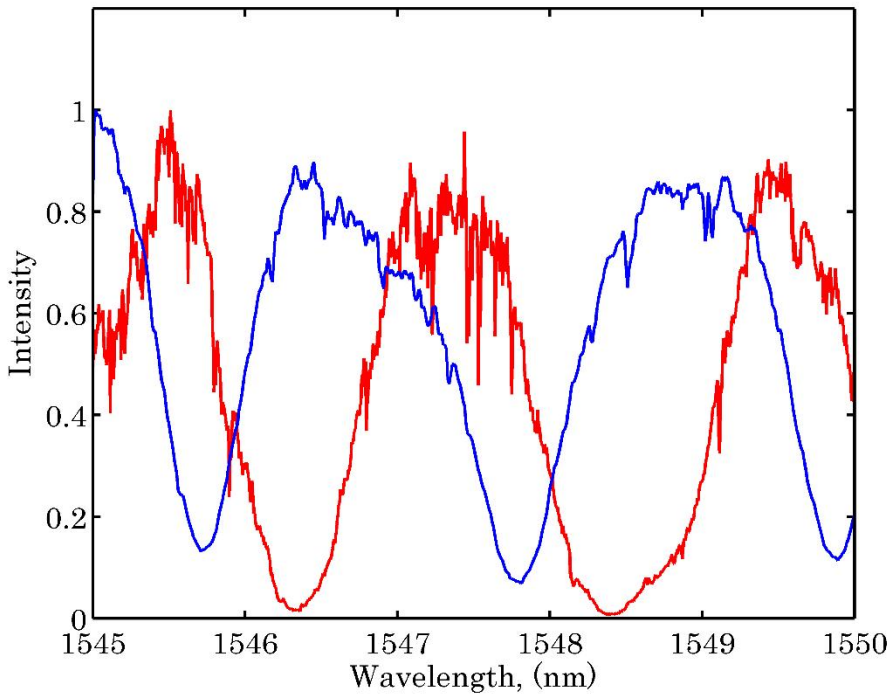

Figure 5.9. Normalized output intensities from both CPAs,

6 CONCLUSIONS

The design of a microring perfect absorber based on laterally coupled optical waveguides was presented. The analytical expressions derived using the coupled mode theory show that for a strong absorption we need a critically coupled microring resonator, i.e., internal losses must me equal in magnitude to the coupling losses. When in the critical coupling condition, absorption can be up to nine orders of magnitude. It can be suppressed just varying the input waves phase difference from 0 to π . This characteristic of controlling the absorption makes the device striking for switching, modulating and sensing applications.

The fabricated device is in good agreement with the analytical results showing an absorption up to 2 orders of magnitude although the system is not critically coupled. With the experimental extracted information we found that the system is 60% critically coupled, being this the main cause for not achieving the strong absorption.

The second CPA with a phase difference between its input waves shows a reduction of the absorption by a 99.8%. Due to the optical design we were not able to measure the output intensity from the left side channel. But this is not a major problem for the device performance.

A direct application in integrated photonics is a modulator. Changing the refractive index of one input waveguide, by injecting current, one can obtain the desired phase difference for achieve an output modulated intensity.

7 REFERENCES

[1] A. Stone, "Gobbling up light with an antilaser," *Physics Today,* vol. 64, p. 68, 2011.

[2] Y. D. Chong, L. Ge, H. Cao and A. D. Stone, "Coherent perfect absorbers: time-reversed lasers," *Phys. Rev. Lett,* vol. 105, p. 053901, 2010.

[3] W. Wan, Y. Chong, L. Ge, H. Noh, A. D. Stone and H. Cao, "Time-Reversed Lasing and Interferometric Control of Absorption," *Science,* vol. 331, p. 889, 2011.

[4] S. Longhi, "PT-symmetric laser absorber," *Phys. Rev. A,* vol. 82, p. 031801, 2010.

[5] H. Noh, Y. Chong, A. D. Stone and H. Cao, " Perfect coupling of light to surface plasmons by coherent absorption," *Phys. Rev. Lett.,* vol. 108, p. 186805, 2012.

[6] V. Klimov, S. Sun and G.-Y. Guo, "Coherent perfect nanoabsorbers based on negative refraction," *Optics Express,* vol. 20, p. 13071, 2012.

[7] H. Noh, S. Popoff and H. Cao, "Broadband subwavelength focusing of light using a passive sink," *Opt Express,* vol. 21, p. 17435, 2013.

[8] M. Albooyeh and C. R. Simovski, "Huge local field enhancement in perfect plasmonic absorbers," *Optics Express,* vol. 20, p. 21888, 2012.

[9] R. Bruck and O. L. Muskens, "Plasmonic nanoantennas as integrated coherent perfect absorbers on SOI waveguides for modulators and all-optical switches," *Optics Express,* vol. 21, p. 27652, 2013.

[10] M. Pu, Q. Feng, C. Hu and X. Luo, "Perfect Absorption of Light by Coherently Induced Plasmon Hybridization in Ultrathin Metamaterial Film," *Plasmonics, 7,4,* vol. 7, p. 733, 2012.

[11] J. Yoon, W. Park, K. Lee, S. Song and R. Magnusson, "Surface-plasmon mediated total absorption of light into silicon," *Opt Express,* vol. 19, p. 20673, 2011.

[12] J. W. Yoon, G. M. Koh, S. H. Song and R. Magnusson, "Measurement and Modeling of a Complete Optical Absorption and Scattering by Coherent Surface Plasmon-Polariton Excitation Using a Silver Thin-Film Grating," *Phys. Rev. Lett. ,* vol. 109, p. 257402, 2012.

[13] C. G. Jianfa Zhang, K. Liu, Z. Zhu, W. Ye, X. Yuan and S. Qin, "Coherent perfect absorption and transparency in a nanostructured graphene film," *Optics Express,* vol. 22, p. 12524, 2014.

[14] S. M. Rao, J. J. F. Heitz, Thomas Roger, Niclas Westerberg and F. Daniele, "Coherent control of light interaction with graphene," *Optics Letters),* vol. 39, p. 5345, 2014.

[15] G. Pirruccio, L. M. Moreno, G. Lozano and J. G. Rivas, "Coherent and Broadband Enhanced Optical Absorption in Graphene”,," *ACS Nano ,* vol. 7, p. 4810, 2013.

[16] J. Z. Song, P. Bai, Z. H. Hang and Y. Lai, "Acoustic coherent perfect absorbers," *New J. Phys.,* vol. 16, p. 033026, 2014.

[17] R. Kakimi, M. Fujita, M. M. Ashida and T. Nagatsuma, "Capture of a terahertz wave in a photonic-crystal slab," *Nature Photonics,* vol. 8, p. 657, 2014.

[18] Gopakumar Ramakrishnan, Gopika K. P. Ramanandan, A. J. L. Adam, M. Xu, N. Kumar, R. W. A. Hendrikx and P. C. M. Planken, "Enhanced terahertz emission by coherent optical absorption in ultrathin semiconductor films on metals," *Optics Express,* vol. 21, p. 16784, 2013.

[19] Y. Shena, L. Shenb, Z. Laia, G. Wangc and X. Dengb, "Time-reversed lasing based on one-dimensional gratings," *Physics Letters A ,* vol. 378, p. 299, 2014.

[20] Z.-R. Zhang, H.-Q. Li, H. Chen, C.-L. Hu and P. Zhou, "Coherent perfect absorption in one-dimensional photonic crystal with a PT-symmetric defect," *EPL,* vol. 105, p. 47008, 2014.

[21] A. Mostafazadeh, "Self-dual spectral singularities and coherent perfect absorbing lasers without PT-symmetry," *J. Phys. A: Math. Theor. ,* vol. 444024, p. 45, 2012.

[22] S. Huang and G. S. Agarwal, "Coherent perfect absorption of path entangled single photons," *Optics Express ,* vol. 22, p. 20936, 2014.

[23] A. Mock, "Low-Power All-Optical Switch Based on Time-Reversed Microring Laser," *Photonics Journal, IEEE,* vol. 4, p. 229, 2012.

[24] R. R. Grote, J. B. Driscoll and a. R. M. Osgood, "Integrated optical modulators and switches using coherent perfect loss," *Optics Letters,* vol. 38, p. 3001, 2013.

[25] B. C. Jacobs and J. D. Franson, "All Optical switching using the quantum Zeno effect and two photon absorption," *Phys. Rev. A,* vol. 79, p. 063830, 2009.

[26] M. Lipson, "Guiding, modulating, and emitting light on Silicon-challenges and opportunities," *Lightwave Technology, Journal of,* vol. 23, p. 4222, 2005.

[27] Max Born and Emil Wolf, Principles of Optics, 4th ed., Oxford: Pergamon Press, 1970, pp. 36-51.

[28] B. E. Little, T. S. Chu, A. H. Haus, J. P. Forsei and J. Laine, "Microring resonator channel dropping filters," *J. Lightwave Technol,* vol. 15, pp. 998-1005, 1997.

[29] A Yariv, "Universal relations for coupling of optical power between microresonators and dielectric waveguides," *Electronics Letters,* vol. 36, 2000.

[30] A. Yariv, "Critical coupling and its control in optical waveguide-ring resonator systems," *IEEE Photonics Technology Letters,* vol. 14, pp. 483-485, 2002.

[31] Q. Xu, B. Schmidt, S. Pradhan and a. M. Lipson, "Micrometre-scale silicon electro-optic modulator," *Nature,* vol. 435, pp. 325-327, 2005.

[32] Y. Vlasov and S. McNab, "Losses in single-mode silicon-on-insulator strip waveguides and bends," *Opt. Express,* vol. 12, pp. 1622-1631, 2004.

[33] N. Sherwood-Droz, H. Wang, L. Chen, B. G. Lee, A. Biberman, K. Bergman and M. Lipson, "Optical 4×4 hitless silicon router for optical Networks-on-Chip (NoC)," *Opt. Express,* vol. 16, pp. 15915-15922, 2008.

[34] Q. Xu, V. R. Almeida and M. Lipson, "Micrometer-scale all-optical wavelength converter on silicon," *Opt. Lett.,* vol. 30, pp. 2733-2735, 2005.

[35] V. R. Almeida, R. R. Panepucci and M. Lipson, "Nanotaper for compact mode conversion," *Opt. Lett.,* vol. 28, pp. 1302-1304, 2003.

[36] W. Hayenga, M. Akhlagui-Bouzan, P.J. Delfyett and M. Khajavikhan, "High finesse silicon ring resonators for monolithic mode-locked lasers," *SPIE,* 2014.

[37] J. T. Verdeyen, Laser electronics, 3rd ed., New Jersey: Prentice Hall International, 1989.

8 APPENDIX A

8.1 Coupled mode theory.

In this appendix the coupling matrix and the coupling parameters are derived based on the coupling of electromagnetic modes. For the approximate solutions of Maxwell's equations for radiation propagating in periodic media, two approaches are generally used, one is the Bloch-wave formalism and the other is the **coupled mode theory.** In the latter theory, the periodic variation of the dielectric tensor is considered as a perturbation that couples the unperturbed normal modes of the structure. In other words, the dielectric tensor as a function of space is written as:

$$\varepsilon(x,y,z) = \varepsilon_0(x,y) + \Delta\varepsilon(x,y,z), \tag{A.1}$$

where $\varepsilon_0(x,y)$ is the unperturbed part of the dielectric tensor, and $\Delta\varepsilon_0(x,y,z)$ is periodic in the z direction and is the only periodically varying part of the dielectric tensor. If we compare Equation. (A.1) with the Fourier expansion of $\varepsilon(x,y,z)$ as in $\varepsilon(\mathbf{x}) = \sum_{\mathbf{G}} \varepsilon_{\mathbf{G}} e^{-i\mathbf{G}\cdot\mathbf{x}}$, then $\varepsilon_0(x,y)$ is the zeroth component of the series and $\Delta\varepsilon(x,y,z)$ contains the rest of the series.

We assume that the normal modes of propagation in the unperturbed dielectric medium described by the dielectric tensor $\varepsilon_0(x,y)$ are known.

Since the unperturbed dielectric medium is homogeneous in the z direction $[\text{i.e., } \partial\varepsilon_0(x,y)/\partial z = 0]$, the normal modes can be written in the form

$$\mathbf{E}_m(x,y)e^{i(\omega t - \beta_m z)}, \tag{A.2}$$

where m is the mode subscript, which can be either continuous for unbound modes, such as plane waves, or discrete for confined modes, such as waveguide modes. These normal modes satisfy

$$\left[\frac{\partial^2}{\partial x^2}+\frac{\partial^2}{\partial x^2}+\omega^2\mu\varepsilon_0(x,y)-\beta_m^2\right]\mathbf{E}_m(x,y)=0. \tag{A.3}$$

If an arbitrary field of frequency ω is excited at $z=0$, the propagation of this field in the unperturbed medium can always be expressed in terms of a linear combination of normal modes,

$$\mathbf{E}=\sum_m A_m\mathbf{E}_m(x,y)e^{i(\omega t-\beta_m z)}, \tag{A.4}$$

where the A_m's are constants. Such as expansion is possible because these normal modes form a complete set. The modes are usually normalized to a power flow of 1 W in the z direction. Thus the orthogonal relation of the modes can be written

$$\frac{1}{2}\int\left(\mathbf{E}_l\times\mathbf{H}_k^*\right)_z dxdy=\delta_{lk}, \tag{A.5}$$

where $\mathbf{H}_k$ is the magnetic field associated with the mode $\mathbf{E}_k$. When $\Delta\bullet\mathbf{E}=0$ and the modes $\mathbf{E}_m$ satisfy Equation (A.3), this orthogonal relation becomes

$$\int\mathbf{E}_k^*(x,y)\cdot\mathbf{E}_l(x,y)dxdy=\frac{2\omega\mu}{|\beta_k|}\delta_{kl}, \tag{A.6}$$

where δ_{kl} is the Kronecker delta for confined modes and the Dirac delta function for unbounded modes. If a single mode is excited at $z=0,$ say $\mathbf{E}_1(x,y)e^{i(\omega t-\beta_1 z)}$ in the perturbed medium described by the dielectric tensor $\varepsilon(x,y,z)=\varepsilon_0(x,y)+\Delta\varepsilon(x,y,z)$. The presence of the dielectric perturbation $\Delta\varepsilon(x,y,z)$ gives rise to a new perturbation polarization

$$\Delta\mathbf{P} = \Delta\varepsilon(x,y,z)\mathbf{E}_1(x,y)e^{i(\omega t-\beta_1 z)}.$$

If this polarization wave, acting as a distributed source, can feed energy into (or out of) some other mode $\mathbf{E}_2(x,y)e^{i(\omega t-\beta_2 z)}$, then we say that the dielectric perturbation $\Delta\varepsilon(x,y,z)$ couples (i.e., causes energy exchange) between modes $\mathbf{E}_1$ and $\mathbf{E}_2$. Let us find next under what conditions this coupling takes place.

The energy exchange between unperturbed modes due to the dielectric perturbation is analogous to a transition between the eigenstates of an atom under the influence of a time-dependent perturbation. The mathematical approach is sometimes called the method of variation of constants. The procedure consists of expressing the electric field vector of the electromagnetic wave as an expansion in the normal modes of the unperturbed dielectric structure, where the expansion coefficients evidently depend on z, since for $\varepsilon_0 \neq 0$ the waves $\mathbf{E}_m(x,y)e^{i(\omega t-\beta_m z)}$, are no longer eigenmodes:

$$\mathbf{E} = \sum_m A_m(z)\mathbf{E}_m(x,y)e^{i(\omega t-\beta_m z)}, \tag{A.7}$$

substituting Equation (A.7) into the wave equation

$$\left\{\nabla^2 + \omega^2\mu\left[\varepsilon_0(x,y) + \Delta\varepsilon(x,y,z)\right]\right\}\mathbf{E} = 0, \tag{A.8}$$

and using Equation (A.3)

$$\left\{\nabla^2 + \omega^2\mu\left[\varepsilon_0(x,y) + \Delta\varepsilon(x,y,z)\right]\right\}\sum_m A_m(z)\mathbf{E}_m(x,y)e^{i(\omega t-\beta_m z)} = 0,$$

obtaining the partials derivatives

$$\frac{\partial^2 \mathbf{E}}{\partial x^2} = \sum_m A_m(z) \frac{\partial^2 \mathbf{E}_m(x,y)}{\partial x^2} e^{i(\omega t - \beta_m z)},$$

$$\frac{\partial^2 \mathbf{E}}{\partial y^2} = \sum_m A_m(z) \frac{\partial^2 \mathbf{E}_m(x,y)}{\partial y^2} e^{i(\omega t - \beta_m z)},$$

$$\frac{\partial \mathbf{E}}{\partial z} = \sum_m \left(\frac{d}{dz} - i\beta_m \right) A_m(z) \mathbf{E}_m(x,y) e^{i(\omega t - \beta_m z)},$$

$$\frac{\partial^2 \mathbf{E}}{\partial z^2} = \sum_m \left(\frac{d^2}{dz^2} - i\beta_m \frac{d}{dz} - i\beta_m \frac{d}{dz} + \left(-\beta_m^2\right) \right) A_m(z) \mathbf{E}_m(x,y) e^{i(\omega t - \beta_m z)},$$

$$\frac{\partial^2 \mathbf{E}}{\partial z^2} = \sum_m \left(\frac{d^2}{dz^2} - i2\beta_m \frac{d}{dz} - \beta_m^2 \right) A_m(z) \mathbf{E}_m(x,y) e^{i(\omega t - \beta_m z)}.$$

The laplacian is of the form:

$$\nabla^2 \mathbf{E} = \sum_m \left[\frac{\partial^2}{\partial x^2} + \frac{\partial^2}{\partial y^2} + \left(\frac{d^2}{dz^2} - i2\beta_m \frac{d}{dz} - \beta_m^2 \right) \right] A_m(z) \mathbf{E}_m(x,y) e^{i(\omega t - \beta_m z)},$$

then the wave equation results:

$$\sum_m \left[\frac{\partial^2}{\partial x^2} + \frac{\partial^2}{\partial y^2} + \left(\frac{d^2}{dz^2} - i2\beta_m \frac{d}{dz} - \beta_m^2 \right) \right] A_m(z) \mathbf{E}_m(x,y) e^{i(\omega t - \beta_m z)}$$
$$+\omega^2 \mu \varepsilon_0(x,y) \sum_m A_m(z) \mathbf{E}_m(x,y) e^{i(\omega t - \beta_m z)}$$
$$+\omega^2 \mu \Delta\varepsilon(x,y,z) \sum_l A_l(z) \mathbf{E}_l(x,y) e^{i(\omega t - \beta_l z)} = 0,$$

rearranging some terms we have:

$$\sum_m \left[\frac{\partial^2}{\partial x^2} + \frac{\partial^2}{\partial y^2} + \omega^2 \mu \varepsilon_0(x,y) - \beta_m^2 \right] A_m(z)\mathbf{E}_m(x,y)e^{i(\omega t - \beta_m z)}$$
$$+ \sum_k \left(\frac{d^2}{dz^2} - i2\beta_k \frac{d}{dz} \right) A_k(z)\mathbf{E}_k(x,y)e^{i(\omega t - \beta_k z)}$$
$$+ \omega^2 \mu \Delta\varepsilon(x,y,z) \sum_l A_l(z)\mathbf{E}_l(x,y)e^{i(\omega t - \beta_l z)} = 0,$$

the first part of the last equation is Equation. (A.3), the expression reduces to:

$$\sum_k \left(\frac{d^2 A_k(z)}{dz^2} - i2\beta_k \frac{dA_k(z)}{dz} \right) \mathbf{E}_k(x,y)e^{-i\beta_k z}$$
$$= -\omega^2 \mu \Delta\varepsilon(x,y,z) \sum_l A_l(z)\mathbf{E}_l(x,y)e^{-i\beta_l z}. \tag{A.9}$$

We now assume further that the dielectric perturbation is "weak", so that the variation of the mode amplitudes is "slow" and satisfies the condition

$$\left| \frac{d^2 A_k(z)}{dz^2} \right| \ll \left| \beta_k \frac{dA_k(z)}{dz} \right|. \tag{A.10}$$

This condition is known as parabolic approximation and is often used when the perturbation is small. Thus, neglecting the second derivative in Equation (A.9) leads to

$$-2i \sum_k \beta_k \left(\frac{dA_k(z)}{dz} \right) \mathbf{E}_k(x,y)e^{-i\beta_k z}$$
$$= -\omega^2 \mu \sum_l \Delta\varepsilon(x,y,z) A_l(z)\mathbf{E}_l(x,y)e^{-i\beta_l z}. \tag{A.11}$$

We next take the scalar product of Equation (A.11) with $\mathbf{E}_k^*(x,y)$ and integrate over x and y.

$$-2i\sum_k \beta_k \left(\frac{dA_k(z)}{dz}\right)\int \mathbf{E}_k^*(x,y)\cdot\mathbf{E}_k(x,y)dxdye^{-i\beta_k z}$$
$$=-\omega^2\mu\sum_l\sum_k A_l(z)\int \mathbf{E}_k^*(x,y)\cdot\Delta\varepsilon(x,y,z)\mathbf{E}_l(x,y)dxdye^{-i\beta_l z},$$

using the orthogonal relation (A.6) we can write:

$$\langle k\,|\,k\rangle\left(\frac{dA_k(z)}{dz}\right)=\frac{2\omega^2\mu}{2i\beta_k}\sum_l A_l(z)\langle k|\Delta\varepsilon|l\rangle e^{i(\beta_k-\beta_l)z}, \qquad \text{(A.12)}$$

where

$$\langle k\,|\,k\rangle=\int \mathbf{E}_k^*(x,y)\cdot\mathbf{E}_k(x,y)dxdy=\frac{2\omega\mu}{|\beta_m|}, \qquad \text{(A.13)}$$

$$\langle k\,|\,\Delta\varepsilon\,|\,l\rangle=\int \mathbf{E}_k^*(x,y)\cdot\Delta\varepsilon(x,y,z)\mathbf{E}_l(x,y)dxdy. \qquad \text{(A.14)}$$

Since the dielectric perturbation $\Delta\varepsilon(x,y,z)$ is periodic in z, we can expand it as a Fourier series

$$\Delta\varepsilon(x,y,z)=\sum_{m\neq 0}\varepsilon_m(x,y)\exp\left[-im\frac{2\pi}{\Lambda}z\right], \qquad \text{(A.15)}$$

where the summation is over all m except $m=0$ because of the definition of $\Delta\varepsilon(x,y,z)$ in Equation A.1. Substitution of Equations (A.15), (A.14), (A.13) in Equation A.12 leads to

$$\frac{dA_k(z)}{dz} = -i\frac{\omega}{4}\frac{|\beta_k|}{\beta_k}\sum_l\sum_m A_l(z)\int \mathbf{E}_k^*(x,y)\cdot\varepsilon_m(x,y)\mathbf{E}_l(x,y)dxdy e^{i(\beta_k-\beta_l-m\frac{2\pi}{\Lambda})z}$$

$$\frac{dA_k(z)}{dz} = -i\frac{|\beta_k|}{\beta_k}\sum_l\sum_m A_l(z)C_{kl}^{(m)}e^{i(\beta_k-\beta_l-m\frac{2\pi}{\Lambda})z}. \qquad \text{(A.16)}$$

where the coupling coefficient $C_{kl}^{(m)}$ is defined as

$$C_{kl}^{(m)} = \int \mathbf{E}_k^*(x,y)\cdot\varepsilon_m(x,y)\mathbf{E}_l(x,y)dxdy, \qquad \text{(A.17)}$$

this coefficient $C_{kl}^{(m)}$ reflects the magnitude of coupling between the k th and the l th modes due to the m th Fourier component of the dielectric perturbation.

Equation A.16 constitutes a set of coupled linear differential equations. In principle, an infinite number of mode amplitudes are involved. However, in practice, especially near the condition of resonant coupling, only two modes are strongly coupled, and Eq. (A.16) reduces to two equations for the two mode amplitudes. By resonant coupling we mean a mode coupling at the condition when

$$\beta_k - \beta_l - m\frac{2\pi}{\Lambda} = 0, \qquad \text{(A.18)}$$

for some integer m. This condition is of fundamental importance, and we will refer to it as "longitudinal phase matching" or just as phase matching. This condition is the spatial analogue of the conservation of energy in time-dependent perturbation theory and therefore may be called the conservation of momentum. The resonant coupling can be explained as follows: by examining the coupled Equation (A.16), we notice that the increment in the field amplitude of the k th mode, dA_k,

due to the mode coupling with the l th mode in the region between z and $z+dz$ via the m th Fourier component of the dielectric perturbation is given by

$$dA_k(z) = -i\frac{|\beta_k|}{\beta_k} C_{kl}^{(m)} A_l(z) \exp\left[i\left(\beta_k - \beta_l - m\frac{2\pi}{\Lambda} \right) z \right] dz, \quad \text{(A.19)}$$

since the field amplitudes are slowly varying functions of space, we may integrate Equation (.19) over a distance which is much larger than the period Λ, yet is much smaller than the variation scale of the field amplitudes. This leads to an expression for the net increment of the field amplitude, ΔA_k, due to mode coupling with l th mode over the distance between z and $z+L$ via the m th Fourier component of the dielectric perturbation:

$$\Delta A_k(z) = -i\frac{|\beta_k|}{\beta_k} C_{kl}^{(m)} A_l(z) \int_{L \gg \Lambda} \exp\left[i\left(\beta_k - \beta_l - m\frac{2\pi}{\Lambda} \right) z \right] dz, \quad \text{(A.20)}$$

from this equation we find that mode coupling between the k th and l th modes is insignificant when the condition (A.18) is not satisfied of some integer m, because the integral (A.20) is non-vanishing only when the exponent is zero, which is exactly the phase-matching condition (A.18)

The propagation of electromagnetic radiation in a periodically perturbed dielectric medium can be described by the method of variation of constants. These mode amplitudes ("constants") are governed by the coupled-mode equations (A.16). For significant mode coupling to take place between modes *k* and *l*, two conditions must be satisfied. The first is expressed by Eq. (A.18), the kinematical condition.

Second, the coupling coefficient, $C_{kl}^{(m)}$, must not vanish. The latter is also called the dynamical condition, since it depends upon characteristics of the waves such as their polarizations and mode profiles.

8.2 Coupled mode equations.

Equation (A.16) describes the most general case of mode coupling due to a periodic dielectric perturbation. In practice, often only the coupling between two modes is involved. Let the two coupled modes be designated as 1 and 2. Neglecting interaction with any of the other modes, the coupled-mode equations become

$$\begin{aligned}\frac{d}{dz}A_1 &= -i\frac{\beta_1}{|\beta_1|}C_{12}^{(m)}A_2\exp(i\Delta\beta z),\\ \frac{d}{dz}A_2 &= -i\frac{\beta_1}{|\beta_1|}C_{21}^{(-m)}A_1\exp(-i\Delta\beta z),\end{aligned} \tag{A.21}$$

where

$$\Delta\beta = \beta_1 - \beta_2 - m\frac{2\pi}{\Lambda}, \tag{A.22}$$

and $C_{12}^{(m)}, C_{21}^{(-m)}$ are the coupling coefficients given by (A.17). It can be shown directly from the definition (A.17) that

$$C_{12}^{(m)} = \left[C_{21}^{(-m)}\right]^*, \tag{A.23}$$

provided that $\Delta\varepsilon(x,y,z)$ is a Hermitian dielectric tensor.

8.3 Codirectional coupling.

When the coupled modes are propagating in the same direction, say the $+z$ direction, the sign factors $\beta_1/|\beta_1|$ and $\beta_2/|\beta_2|$ are both equal to 1. The coupled equations become

$$\begin{aligned}\frac{d}{dz}A_1 &= -i\kappa A_2 e^{i\Delta\beta z},\\ \frac{d}{dz}A_2 &= -i\kappa^* A_1 e^{-i\Delta\beta z},\end{aligned} \tag{A.24}$$

where

$$\kappa = C_{12}^{(m)}. \tag{A.25}$$

Remember that A_1 and A_2 are the complex amplitudes of the normalized modes. Therefore $|A_1|^2$ and $|A_2|^2$ represent the power flow in modes 1 and 2, respectively. The coupled mode equations (A.24) are consistent with the conservation of energy, which requires that

$$\frac{d}{dz}\left\{|A_1|^2 + |A_2|^2\right\} = 0.$$

Next we are going to solve the system (A.24). First we propose two fields of the form $a_1(z) = A_1(z)\exp\left[-i\Delta\beta z/2\right]$ and $a_2(z) = A_2(z)\exp\left[i\Delta\beta z\right]$, taking the derivative of these fields leads:

$$\begin{aligned}\frac{da_1(z)}{dz} &= \frac{dA_1(z)}{dz}\left(\exp\left[-i\frac{\Delta\beta z}{2}\right]\right) - i\frac{\Delta\beta}{2}A_1(z)\exp\left[-i\frac{\Delta\beta z}{2}\right],\\ \frac{da_2(z)}{dz} &= \frac{dA_2(z)}{dz}\left(\exp\left[i\frac{\Delta\beta z}{2}\right]\right) + i\frac{\Delta\beta}{2}A_2(z)\exp\left[-i\frac{\Delta\beta z}{2}\right],\end{aligned} \tag{A.26}$$

substituting Equation (A.24) in (A.26)

$$\begin{aligned}\frac{da_1(z)}{dz} &= -i\kappa A_2(z)e^{i\frac{\Delta\beta z}{2}} - i\frac{\Delta\beta}{2}A_1(z)e^{-i\frac{\Delta\beta}{2}z},\\ \frac{da_2(z)}{dz} &= -i\kappa^* A_1(z)e^{-i\frac{\Delta\beta z}{2}} + i\frac{\Delta\beta}{2}A_2(z)e^{i\frac{\Delta\beta}{2}z},\end{aligned} \tag{A.27}$$

Equation (A.27) can be written in matrix form

$$\frac{d}{dz}\begin{pmatrix} a_1(z) \\ a_2(z) \end{pmatrix} = \begin{pmatrix} -i\frac{\Delta\beta}{2} & -i\kappa \\ -i\kappa^* & i\frac{\Delta\beta}{2} \end{pmatrix}\begin{pmatrix} a_1(z) \\ a_2(z) \end{pmatrix}, \tag{A.28}$$

$$\frac{d\mathbf{a}}{dz} = \mathbf{M}\mathbf{a}.$$

The eigenvalues of $\mathbf{M}$ are found by solving the equation $|\mathbf{M} - \lambda\mathbf{I}| = 0$, where $\mathbf{I}$ is the identity matrix

$$\det\begin{pmatrix} -i\frac{\Delta\beta}{2} - \lambda & -i\kappa \\ -i\kappa^* & i\frac{\Delta\beta}{2} - \lambda \end{pmatrix} = 0,$$

$$\left(-i\frac{\Delta\beta}{2} - \lambda\right)\left(i\frac{\Delta\beta}{2} - \lambda\right) + \kappa^*\kappa = 0,$$

$$\lambda^2 + \left(\tfrac{\Delta\beta}{2}\right)^2 + \kappa^*\kappa = 0,$$

solving for λ we obtain,

$$\lambda_{1,2} = \pm i\sqrt{\left(\tfrac{\Delta\beta}{2}\right)^2 + \kappa^*\kappa},$$
$$\lambda_{1,2} = \pm is,$$

where $s^2 = \left(\tfrac{\Delta\beta}{2}\right)^2 + \kappa^*\kappa$

For finding the eigenvectors, $\mathbf{v}_{1,2}$, of $\mathbf{M}$ we need to solve the equation $\mathbf{M}\mathbf{v}_{1,2} = \pm is\mathbf{v}_{1,2}$.

So, for the eigenvalue is we have

$$\begin{pmatrix} -i\frac{\Delta\beta}{2} & -i\kappa \\ -i\kappa^* & i\frac{\Delta\beta}{2} \end{pmatrix}\begin{pmatrix} v_{11} \\ v_{12} \end{pmatrix} = is\begin{pmatrix} v_{11} \\ v_{12} \end{pmatrix},$$
$$-\tfrac{\Delta\beta}{2s}v_{11} - \tfrac{\kappa}{s}v_{12} = v_{11}, \tag{A.29}$$
$$-\tfrac{\kappa^*}{s}v_{11} + \tfrac{\Delta\beta}{2s}v_{12} = v_{12},$$

Giving a value for v_{12}, here we chose $v_{12}=1$, using this value yields to

$$v_{11}=\tfrac{s}{\kappa^*}\left(\tfrac{\Delta\beta}{2s}-1\right),$$

so the eigenvector $\mathbf{v}_1$ is

$$\mathbf{v}_1=\begin{pmatrix}\tfrac{s}{\kappa^*}\left(\tfrac{\Delta\beta}{2s}-1\right)\\ 1\end{pmatrix}. \tag{A.30}$$

In a similar way as for $\mathbf{v}_1$ we find out the eigenvector $\mathbf{v}_2$

$$\mathbf{v}_2=\begin{pmatrix}\tfrac{s}{\kappa^*}\left(\tfrac{\Delta\beta}{2s}+1\right)\\ 1\end{pmatrix}, \tag{A.31}$$

the general solution of Equation (A.28) is

$$\mathbf{a}=Ae^{isz}\mathbf{v}_1+Be^{-isz}\mathbf{v}_2 \tag{A.32}$$

where A and B are constants. Substituting Equations (A.30) and (A.31) in (A.32) leads to the solution.

$$\begin{aligned}\begin{pmatrix}a_1\\ a_2\end{pmatrix}&=Ae^{isz}\begin{pmatrix}\tfrac{s}{\kappa^*}\left(\tfrac{\Delta\beta}{2s}-1\right)\\ 1\end{pmatrix}+Be^{-isz}\begin{pmatrix}\tfrac{s}{\kappa^*}\left(\tfrac{\Delta\beta}{2s}+1\right)\\ 1\end{pmatrix},\\ a_1&=A\tfrac{s}{\kappa^*}\left(\tfrac{\Delta\beta}{2s}-1\right)e^{isz}+B\tfrac{s}{\kappa^*}\left(\tfrac{\Delta\beta}{2s}+1\right)e^{-isz},\\ a_2&=Ae^{isz}+Be^{-isz},\end{aligned} \tag{A.33}$$

using the initial conditions

$$\begin{aligned}a_1(0)&=A_1(0),\\ a_2(0)&=A_2(0),\end{aligned} \tag{A.34}$$

we can find the constants.

$$\begin{aligned}a_1(0)&=A\tfrac{s}{\kappa^*}\left(\tfrac{\Delta\beta}{2s}-1\right)+B\tfrac{s}{\kappa^*}\left(\tfrac{\Delta\beta}{2s}+1\right)=A_1(0),\\ a_2(0)&=A+B=A_2(0),\end{aligned} \tag{A.35}$$

solving for A and B we find

$$\begin{aligned} A &= \tfrac{A_2(0)}{2} - \tfrac{A_1(0)}{2}\tfrac{\kappa^*}{s} + \tfrac{A_2(0)}{2}\tfrac{\Delta\beta}{2s}, \\ B &= \tfrac{A_2(0)}{2} + \tfrac{A_1(0)}{2}\tfrac{\kappa^*}{s} - \tfrac{A_2(0)}{2}\tfrac{\Delta\beta}{2s}, \end{aligned} \tag{A.36}$$

substituting Equation (A.36) in (A.33) we have

$$\begin{aligned} a_1(z) &= \left(\tfrac{A_2(0)}{2} - \tfrac{A_1(0)}{2}\tfrac{\kappa^*}{s} + \tfrac{A_2(0)}{2}\tfrac{\Delta\beta}{2s}\right)\tfrac{s}{\kappa^*}\left(\tfrac{\Delta\beta}{2s} - 1\right)e^{isz} \\ &\quad + \left(\tfrac{A_2(0)}{2} + \tfrac{A_1(0)}{2}\tfrac{\kappa^*}{s} - \tfrac{A_2(0)}{2}\tfrac{\Delta\beta}{2s}\right)\tfrac{s}{\kappa^*}\left(\tfrac{\Delta\beta}{2s} + 1\right)e^{-isz}, \\ a_2(z) &= \left(\tfrac{A_2(0)}{2} + \tfrac{A_1(0)}{2}\tfrac{\kappa^*}{s} - \tfrac{A_2(0)}{2}\tfrac{\Delta\beta}{2s}\right)e^{isz} \\ &\quad + \left(\tfrac{A_2(0)}{2} + \tfrac{A_1(0)}{2}\tfrac{\kappa^*}{s} - \tfrac{A_2(0)}{2}\tfrac{\Delta\beta}{2s}\right)e^{-isz}. \end{aligned} \tag{A.37}$$

Equation (A.37) reduces to

$$\begin{aligned} a_1(z) &= \left(\cos sz - i\tfrac{\Delta\beta}{2s}\sin sz\right)A_1(0) - i\tfrac{\kappa}{s}\sin szA_2(0), \\ a_2(z) &= -i\tfrac{\kappa^*}{s}\sin szA_1(0) + \left(\cos sz + i\tfrac{\Delta\beta}{2s}\sin sz\right)A_2(0), \end{aligned}$$

so, the solution of Equation (A.24) is

$$\begin{aligned} A_1(z) &= e^{i\frac{\Delta\beta}{2}z}\left\{\left[\cos sz - i\tfrac{\Delta\beta}{2s}\sin sz\right]A_1(0) - i\tfrac{\kappa}{s}\sin szA_2(0)\right\}, \\ A_2(z) &= e^{-i\frac{\Delta\beta}{2}z}\left\{-i\tfrac{\kappa^*}{s}\sin szA_1(0) + \left[\cos sz + i\tfrac{\Delta\beta}{2s}\sin sz\right]A_2(0)\right\}, \end{aligned} \tag{A.38}$$

where $A_1(0)$ is the amplitude of mode 1 at $z=0$, $A_2(0)$ is the amplitude of mode 2 at $z=0$, $A_1(z)$ and $A_2(z)$ are the amplitudes of the coupled modes 1 and 2. As was said before, coupling takes place only at the phase matching condition, $\Delta\beta = 0$, so equation (A.38) reduces to

$$\begin{aligned} A_1(z) &= \cos\left(|\kappa|z\right)A_1(0) - i\sin\left(|\kappa|z\right)A_2(0), \\ A_2(z) &= -i\sin\left(|\kappa|z\right)A_1(0) + \cos\left(|\kappa|z\right)A_2(0). \end{aligned} \tag{A.39}$$

If we define $\theta = |\kappa| z$, where $|\kappa|$ is the magnitude of the coupling factor and z is the coupling distance. So the mode amplitudes can be written in the form of matrix

$$\begin{pmatrix} A_1' \\ A_2' \end{pmatrix} = \begin{pmatrix} \cos\theta & -i\sin\theta \\ -i\sin\theta & \cos\theta \end{pmatrix} \begin{pmatrix} A_1 \\ A_2 \end{pmatrix}, \tag{A.40}$$

here $A_1' = A_1(z), A_2' = A_2(z)$ and $A_1 = A_1(0), A_2 = A_2(0)$.

Equation A.40 describes the amplitude of each mode after the coupling distance z.